JGR Earth Surface

RESEARCH ARTICLE
10.1029/2024JF008219

Functional Regression for Space-Time Prediction of Precipitation-Induced Shallow Landslides in South Tyrol, Italy

Mateo Moreno[1], Luigi Lombardo[1], Stefan Steger[2], Lotte de Vugt[3], Thomas Zieher[4], Alice Crespi[5], Francesco Marra[6], Cees van Westen[1], and Thomas Opitz[7]

[1]Faculty of Geo-Information Science and Earth Observation (ITC), University of Twente, Enschede, The Netherlands, [2]GeoSphere Austria, Vienna, Austria, [3]Department of Geography, University of Innsbruck, Innsbruck, Austria, [4]Austrian Research Centre for Forests (BFW), Innsbruck, Austria, [5]Center for Climate Change and Transformation, Eurac Research, Bolzano, Italy, [6]Department of Geosciences, University of Padova, Padova, Italy, [7]Biostatistics and Spatial Processes, INRAE, Avignon, France

Key Points:

- We integrated static scalar and dynamic functional controls to predict shallow landslides in space and time
- The functional regression framework accounts for errors in the landslide data, has a high performance, and maintains model interpretability
- Our approach can be potentially used for hindcasting, nowcasting, and predicting landslide occurrence under what-if precipitation scenarios

Supporting Information:

Supporting Information may be found in the online version of this article.

Correspondence to:

M. Moreno,
m.morenozapata@utwente.nl

Citation:

Moreno, M., Lombardo, L., Steger, S., de Vugt, L., Zieher, T., Crespi, A., et al. (2025). Functional regression for space-time prediction of precipitation-induced shallow landslides in South Tyrol, Italy. *Journal of Geophysical Research: Earth Surface*, *130*, e2024JF008219. https://doi.org/10.1029/2024JF008219

Received 12 DEC 2024
Accepted 26 MAR 2025

Author Contributions:

Conceptualization: Mateo Moreno, Luigi Lombardo, Stefan Steger
Data curation: Mateo Moreno, Alice Crespi, Francesco Marra
Formal analysis: Mateo Moreno, Thomas Opitz
Methodology: Mateo Moreno, Luigi Lombardo, Thomas Opitz
Supervision: Luigi Lombardo, Stefan Steger, Cees van Westen
Validation: Mateo Moreno
Visualization: Mateo Moreno
Writing – original draft: Mateo Moreno

Abstract Landslides are geomorphic hazards in mountainous terrains across the globe, driven by a complex interplay of static and dynamic controls. Data-driven approaches have been employed to assess landslide occurrence at regional scales by analyzing the spatial aspects and time-varying conditions separately. However, the joint assessment of landslides in space and time remains challenging. This study aims to predict the occurrence of precipitation-induced shallow landslides in space and time within the Italian province of South Tyrol (7,400 km^2). We introduce a functional predictor framework where precipitation is represented as a continuous time series, in contrast to conventional approaches that treat precipitation as a scalar predictor. Using hourly precipitation data and past landslide occurrences from 2012 to 2021, we implemented a functional generalized additive model to derive statistical relationships between landslide occurrence, various static scalar factors, and the preceding hourly precipitation as a functional predictor. We evaluated the resulting predictions through several cross-validation routines, yielding performance scores frequently exceeding 0.90. To demonstrate the model predictive capabilities, we performed a hindcast for a storm event in the Passeier Valley on 4–5 August 2016, capturing the observed landslide locations and illustrating the hourly evolution of the predicted probabilities. Compared to standard early warning approaches, this framework eliminates the need to predefine fixed time windows for precipitation aggregation while inherently accounting for lagged effects. By integrating static and dynamic controls, this research advances the prediction of landslides in space and time for large areas, addressing seasonal effects and underlying data limitations.

Plain Language Summary Landslides are natural hazards in mountainous regions and are often triggered by intense and prolonged precipitation. Predicting where and when landslides may occur is crucial for developing early warning systems, which can help reduce the impacts these processes pose to communities, infrastructure, and the environment. This research uses an innovative method to predict precipitation-induced landslides across space and time in South Tyrol, Italy. Our approach relies on hourly precipitation data and records of past landslides. Unlike traditional approaches, our approach integrates static factors such as lithology, land cover, and topography along with dynamic factors by leveraging precipitation time series. Additionally, our model accounts for seasonal effects and errors in the landslide data, resulting in high performance scores. We tested our model on the landslides triggered during the storm event in the Passeier Valley on 4–5 August 2016, simulating their locations and hourly occurrence probabilities. By enhancing our ability to predict landslides, this research is a contribution toward safer communities and more effective land management practices, ultimately saving lives and reducing losses.

1. Introduction

Landslides are ubiquitous geomorphic hazards in mountainous regions across the globe, resulting in substantial annual economic, societal, and environmental consequences along with fatalities (Froude & Petley, 2018; Kirschbaum et al., 2015; Nadim et al., 2006). Climate change and environmental shifts point to growing landslide hazards of particularly fast-moving, rainfall-induced landslides (Gariano & Guzzetti, 2016; IPCC, 2022; Jakob, 2022; Maraun et al., 2022; Ozturk et al., 2022). Reliable landslide predictions are foundational for landslide early warning systems (LEWS) and can help reduce the impacts of landslides. Thus, ensuring reliable

Writing – review & editing: Luigi Lombardo, Stefan Steger, Lotte de Vugt, Thomas Zieher, Alice Crespi, Francesco Marra, Cees van Westen, Thomas Opitz

predictions of landslides and their resultant impacts is paramount. Nevertheless, the success of such predictions is intrinsically linked to a comprehensive understanding of the underlying factors driving slope instability (Glade et al., 2012).

The causes of landslides arise from a complex interplay between predisposing, preparatory, and triggering environmental factors. Predisposing factors, such as topography and material properties, represent static ground conditions (over the timescales relevant to this process), rendering a location more or less susceptible to landsliding. On the other hand, preparatory and triggering factors, such as precipitation and snowmelt, reflect the dynamic conditions that may either substantially influence the stability of a slope or directly initiate the slope movement (Crozier, 1986; Glade et al., 2012). Therefore, adequate integration of the static and dynamic controls is critical to achieving reliable landslide assessments (Corominas et al., 2014; Westen et al., 2006).

Assessing landslides inherently depends on the scale of the analysis, the purpose, and data availability and quality (Aleotti & Chowdhury, 1999; Fell et al., 2008; Glade et al., 2012; Guzzetti et al., 2005; Westen et al., 2008). For regional-scale assessments, data-driven models are widely used to evaluate both the spatial aspect—determining "where" landslides may likely occur—and the temporal aspect—determining "when" landslides may likely occur. Data-driven landslide susceptibility models address the spatial component by deriving statistical relationships between past landslide occurrences and a set of static environmental factors, enabling the estimation of the spatial propensity of an area to experience slope instabilities (Alvioli et al., 2024; Bryce et al., 2024; Elia et al., 2023; Goetz et al., 2015; Opitz et al., 2022; Tanyas et al., 2019). The resulting maps are frequently used and considered relevant in land use and spatial planning. Limitations in the applicability of these models arise, given that the landslide inventories rarely provide complete representations of past landslides, and strategies to account for them are rarely implemented (Bornaetxea et al., 2018; Knevels et al., 2020; Lima et al., 2021; Steger et al., 2021).

The temporal component is linked to the assessment of the dynamic triggering factors. In our case, Italy, precipitation was identified as the primary factor influencing the timing of shallow landslide occurrence (Brunetti et al., 2010). In this context, data-driven approaches are applied to elaborate on critical triggering conditions, with empirical precipitation or rainfall thresholds commonly used to predict landslide occurrence (Gariano et al., 2015; Niyokwiringirwa et al., 2024; Peruccacci et al., 2017; Segoni et al., 2018). These thresholds are derived by linking past landslide occurrence data with associated precipitation measures (e.g., rainfall intensity and duration, cumulative storm or event rainfall and duration) and serve as foundations for early warnings (Gariano et al., 2015; Guzzetti et al., 2020). These methods frequently focused on the triggering precipitation conditions, and comparatively few studies address the effects of preparatory factors and hydrological effects (Bogaard & Greco, 2016; Greco et al., 2023; Monsieurs et al., 2019; Steger et al., 2023).

Joint assessment of spatial and temporal aspects in landslide modeling is seldomly addressed in the literature, though recent studies highlight its promising potential (Ahmed et al., 2023; Bajni et al., 2023; Caleca et al., 2024; Knevels et al., 2020; Moreno et al., 2024; Steger et al., 2024). These approaches integrate static and dynamic landslide controls as scalar values, such as precipitation (Wang et al., 2022), soil moisture (Stanley et al., 2021), ground motion (Dahal, Tanyas, van Westen, et al., 2024), temperature (Loche et al., 2022), and snowmelt (Camera et al., 2021), by dissecting the temporal component and aggregating dynamic predictors over time (e.g., years, seasons, months, days, or hours). For instance, in Wang et al. (2022), landslide probabilities were estimated over a 31-year period by clustering the landslide inventory according to the designated year of occurrence and analyzing different rainfall metrics for each year. Similarly, in Dahal, Tanyas, and Lombardo (2024), the authors developed seasonal landslide predictive models by incorporating various rainfall and ground motion metrics, using the landslide inventories mapped due to the Gorkha earthquake in 2015 and the pre-monsoon and post-monsoon seasons in the subsequent years. In Steger et al. (2024), a dynamic shallow landslide model was devised by integrating static ground conditions with cumulative daily precipitation, expressed as medium-term preparatory and short-term triggering precipitation. Lombardo et al. (2020) developed a Bayesian model for space-time trends in a century-spanning observation data set for the Collazzone area, Italy, by combining static predictors with random effects representing unobserved environmental triggers, such as extreme precipitation events. In Knevels et al. (2020), by combining data from weather stations and ground-based radar, 3-hr rainfall intensity and 5-day antecedent rainfall were used along with static factors to assess the landslide triggered after a particular storm event.

A relevant issue arises when using scalar values to aggregate dynamic properties over time, as this approach overlooks the potential insights a data-driven model could derive from information on the entire time series. To date, relatively few studies have focused on integrating static and dynamic factors while leveraging the functional nature of dynamic predictors, with most prioritizing performance over interpretability. For example, in Fang et al. (2023), a deep learning architecture initially designed for speech recognition was applied to incorporate daily rainfall time series in a landslide predictive model. This resulted in a substantial improvement in predictive power of ∼20% compared to models that rely on scalar rainfall representations. Lim et al. (2024) extended the findings of Fang et al. (2023) by testing a different deep learning architecture in a data-scarce environment using daily rainfall, reporting similar enhanced performances. In another study, Dahal, Tanyas, and Lombardo (2024) considered ground motion as a functional predictor alongside static controls to predict landslide occurrence, achieving an improvement of 16% in the predictive capabilities compared to a model using only scalar inputs.

This study focuses on space-time shallow landslide modeling. We build upon previous work detailed in Moreno et al. (2024) and Steger et al. (2024), where analyses were performed in the Italian province of South Tyrol and covered a 21-year period (2000–2020). In their work, Moreno et al. (2024) implemented a space-time classifier equipped with static and dynamic predictors, the latter being expressed through precipitation data. Their model was based on the slope unit and features the precipitation signal in a scalar form—daily precipitation and its cumulative expression over time. Similarly, Steger et al. (2024) conducted an analogous experiment, sharing the same study area and technique. Nevertheless, they explored a different mapping unit (grid cells), refined sampling strategies, and extended the analysis to derive dynamic probability thresholds for early warning purposes. Our work extends these two research lines by covering a 10-year period (2012–2021) while also accounting for errors in the available landslide data, providing interpretable results, and demonstrating the practical application through hindcasting the landslides triggered by a storm event in the study area. However, we explore a different modeling archetype that has never appeared in landslide science to date. This is based on functional regression, a statistical method whose implementation allowed us to regress (a) a scalar response expressed as landslide presence and absence against the (b) continuous hourly precipitation time series rather than their scalar aggregation in time. Together with this functional predictor, we also integrated static ones into the model and ultimately tested it for simulation. We recall that standard landslide early warnings are issued on the basis of models that make use of the precipitation information aggregated into single values. In contrast, the underlying assumption of the present work is that a continuous representation of the precipitation signal may bring much more information, thus ultimately improving the predictions. In summary, the key distinction between this contribution and previous work lies in the treatment of the precipitation data—not as discrete scalar values but as a continuous function over time.

In the remainder of the paper, Section 2 outlines the study area, while Section 3 outlines the landslide data, and the environmental predictors we use in our analysis. Section 4 provides the necessary background on the functional regression framework along with the data sampling strategy, feature extraction, and model validation approaches. Section 5 presents the key results, focusing on the data sampling, the model interpretation, and applicability. Finally, we discuss the findings, including a comparison with a benchmark model, and conclude in Sections 6 and 7 with an outlook on future research directions.

2. Study Area

Located in the Eastern Alps, South Tyrol covers about 7,400 km^2, constituting the northernmost province of Italy. Its landscape is characterized by substantial heterogeneity in geomorphology, geology, land cover, and climate. The altitudinal gradient ranges from ∼3,900 m above sea level (a.s.l.) in the highest peaks to ∼200 m a.s.l. in the narrow valley bottoms (see Figure 1). The geological settings are marked by the Periadriatic Line, the major tectonic fault that delineates the metamorphic-dominated Austroalpine section from the carbonate sedimentary-dominated Southalpine section (Stingl & Mair, 2005). The land use consists of ∼40% forest, mainly on hillsides, ∼35% agricultural land, prevalent in flat terrain, and the remaining ∼25% corresponds to unproductive land (Autonomous Province of South Tyrol, 2021). The climate conditions exhibit strong seasonal and spatial variations, with mean annual precipitation spanning from ∼500 mm in the western inner valleys to ∼1,500 mm in the northern and northeastern highlands. Seasonal variation manifests in the wettest months during summer and in the driest months during winter. The mean annual temperature ranges from approximately +15°C in the southern lowlands to around −10°C on the highest peaks, with the warmest conditions occurring in July, while the coldest ones arise in January (Crespi et al., 2021).

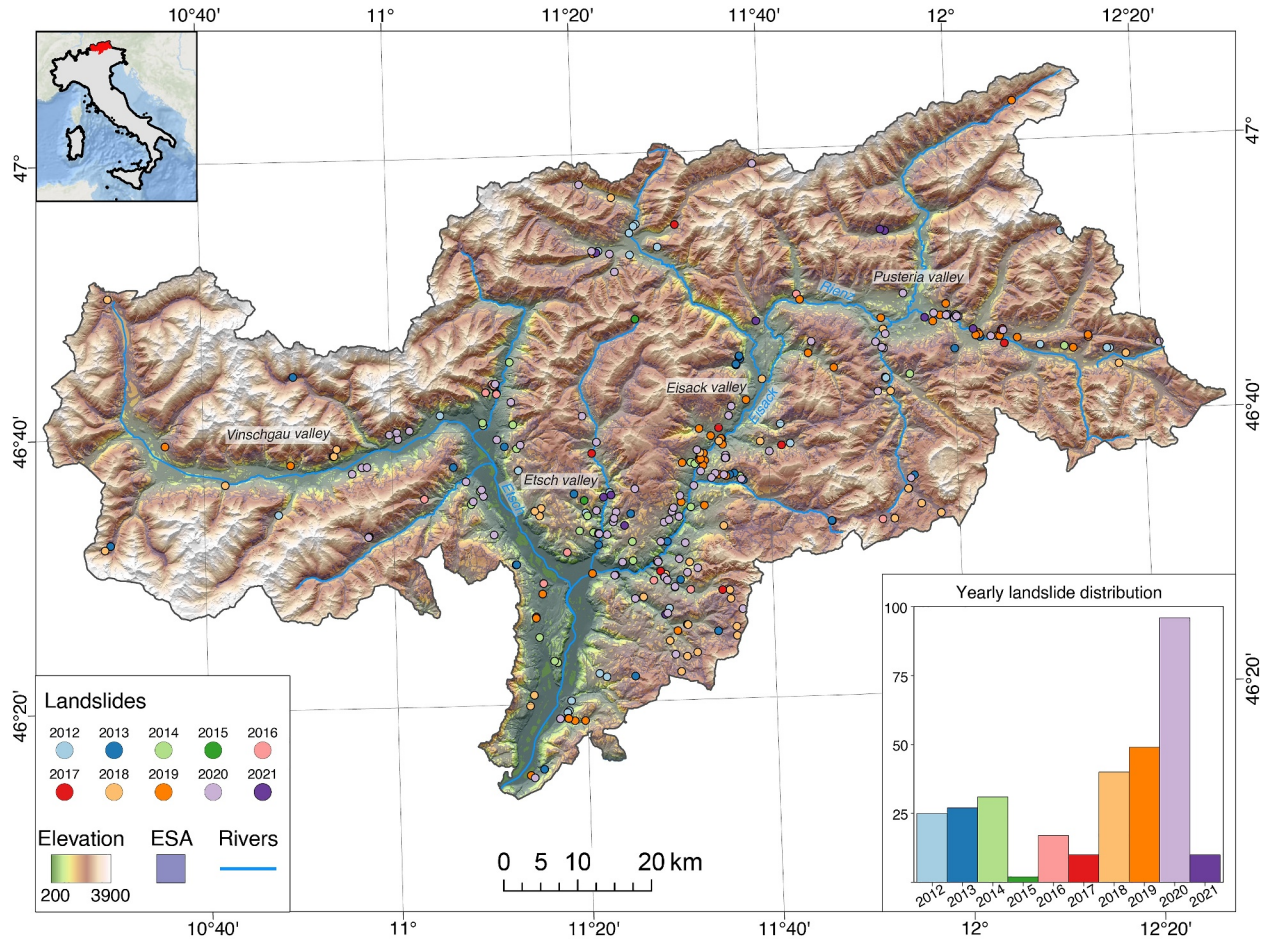

Figure 1. Study area showing the elevation and the distribution of the filtered landslide scarp locations throughout the years ($n = 307$). The dark mask corresponds to the effectively surveyed area, as explained in Section 4.

The specified physiographical attributes render South Tyrol predisposed to landslides, with a predominant occurrence of falls, slides, and flows. In terms of shallow slides, previous research highlighted intense or prolonged precipitation as the main triggering factors, but topography, material, vegetation cover, and land use also contribute to slope instability (de Vugt et al., 2024; Moreno et al., 2024; Piacentini et al., 2012; Schlögel et al., 2020; Steger et al., 2023; Tasser et al., 2003).

3. Data

3.1. Landslide Inventory

This study relies on data sourced from the Italian landslide inventory (Inventario dei Fenomeni Franosi in Italia; IFFI) accessible through the IdroGeo platform (Iadanza et al., 2021a; Iadanza et al., 2021b; https://idrogeo.isprambiente.it/). In South Tyrol, the point-based information explicitly denotes the locations of field-mapped landslide scarps (Trigila et al., 2010). As of the latest access in November 2022, the inventory documented 11,944 landslides, with roughly 40% categorized as falls/topples, 35% as slides, and 15% as flows. As described in Steger et al. (2021), the landslide data systematically captures damage-causing and infrastructure-threatening events that prompted intervention by the provincial authorities, while events without such interventions are usually not reported. This spatial bias in the data results in landslide occurrences being underrepresented in locations far from infrastructure. If not addressed, such bias can propagate and significantly affect the final modeling outcomes, undermining their reliability and practical applicability. Therefore, we implemented a strategy to account for the inherent bias present in the landslide data, as detailed in Section 4.1. On the other hand, the IFFI inventory contains a comprehensive set of attributes, several of which are leveraged in this analysis, as

explained in Section 4.1. Among the most relevant for the analyses presented here is the triggering date, which is recorded at varying levels of temporal precision for each record, ranging from the year, month, and day of occurrence. However, it is important to note that the hour of occurrence is not included in the data set.

Additionally, an independent landslide inventory mapped by de Vugt et al. (2024) from high-resolution space-borne remote sensing information was considered. The 55 landslide entries were generated using multispectral imagery by PlaneScope and RapidEye to investigate the mass movements triggered by a storm event on 4–5 August 2016 in the Passeier Valley, a basin located in the northwestern part of the study area.

3.2. Geo-Environmental Factors

3.2.1. Static Factors

Identifying areas prone to landsliding through data-driven approaches hinges on analyzing spatial environmental variables observed at locations with landslides and those without. Numerous contributions have elaborated on understanding the different predisposing factors and their role in slope instability (Reichenbach et al., 2018). For this study, we focused on predictors whose interpretation can provide insights into the shallow landsliding processes. Two morphometric variables were derived from a resampled lidar-DTM at a 30 × 30 m spatial resolution. Slope steepness, a key variable in landslide susceptibility modeling, captures the gravitational forces influencing the sliding potential (Budimir et al., 2015; Westen et al., 2008). The relative elevation indicates altitude-dependent environmental and climatic conditions associated with slope instability; therefore, it is quantified via the standardized height provided in SAGA GIS (Conrad et al., 2015; Dietrich & Böhner, 2008). The standardized height quantifies the relative topographic position along a hillslope. Besides the vertical offset of an individual grid cell, this metric accounts for the spatial extent of the associated catchment area, so it not only relates to the adjacent channel and crest lines but also comprises the widespread topology (Böhner & Selige, 2006). Lithology to describe the underlying material composition was extracted from a regional geological map illustrating five main classes: crystalline, porphyry, sedimentary, plutonic, and calcschist ("Geologische Übersichtskarte Südtirol"; Geokatalog, 2019). A proxy for vegetation effects is the land cover grouped into six classes: agriculture, forest, infrastructure, pasture, rock, and water/glacier ("Realnutzungskarte Südtirol v. 2015"; Geokatalog, 2019). This map was subsequently used to create a binary forest cover map by extracting the forest class (1) and setting the remaining classes as no forest (0). Ultimately, mean annual precipitation from 2000 to 2020, derived from the daily precipitation grids in Crespi et al. (2021), was used to capture the overall climatic patterns and describe relatively drier and wetter areas.

3.3. Dynamic Factors—Gridded Precipitation Data

Hourly precipitation data were extracted from the Integrated Nowcasting through Comprehensive Analysis (INCA; Haiden et al., 2011) publicly released by GeoSphere Austria. INCA is a multivariable analysis and nowcasting system that offers near-real-time analyses and forecasts of variables such as precipitation, temperature, wind, humidity, and cloudiness. The INCA precipitation analysis, available since March 2011, provides data on a 1 km × 1 km spatial grid with a 15-min temporal resolution. It integrates inputs from ∼250 semi-automated weather stations, five Austrian C-band radars, and high-resolution topography. Although the precipitation measurements primarily reflect rainfall, they may also include snowfall during winter. The data set used in this research was accessed via the GeoSphere Austria web platform (https://data.hub.geosphere.at/dataset/inca-v1-1h-1km) at a 1-hr temporal resolution. For more details on the generation and processing of the INCA precipitation analysis product, refer to Ghaemi et al. (2021) and Haiden et al. (2011). One of the key advantages of using a spatially distributed nowcasting system with high-resolution radar input is its ability to provide a more accurate spatial representation of precipitation. This is critical for effectively assigning the precipitation time series and designing our modeling framework, as highlighted by Marra et al. (2014, 2016).

4. Methods

The methodical workflow is shown in Figure 2, with details outlined in Sections 4.1 to 4.4. Our model is based on binary data (i.e., landslide presences and absences), which is why the first step, data sampling, consisted of filtering the information from the landslide inventory (i.e., landslide presences) and strategically selecting the landslide absences. This selection included generating the effectively surveyed area (ESA; Bornaetxea et al., 2018) to spatially constrain the absence of sampling to well-investigated and non-trivial terrain. The

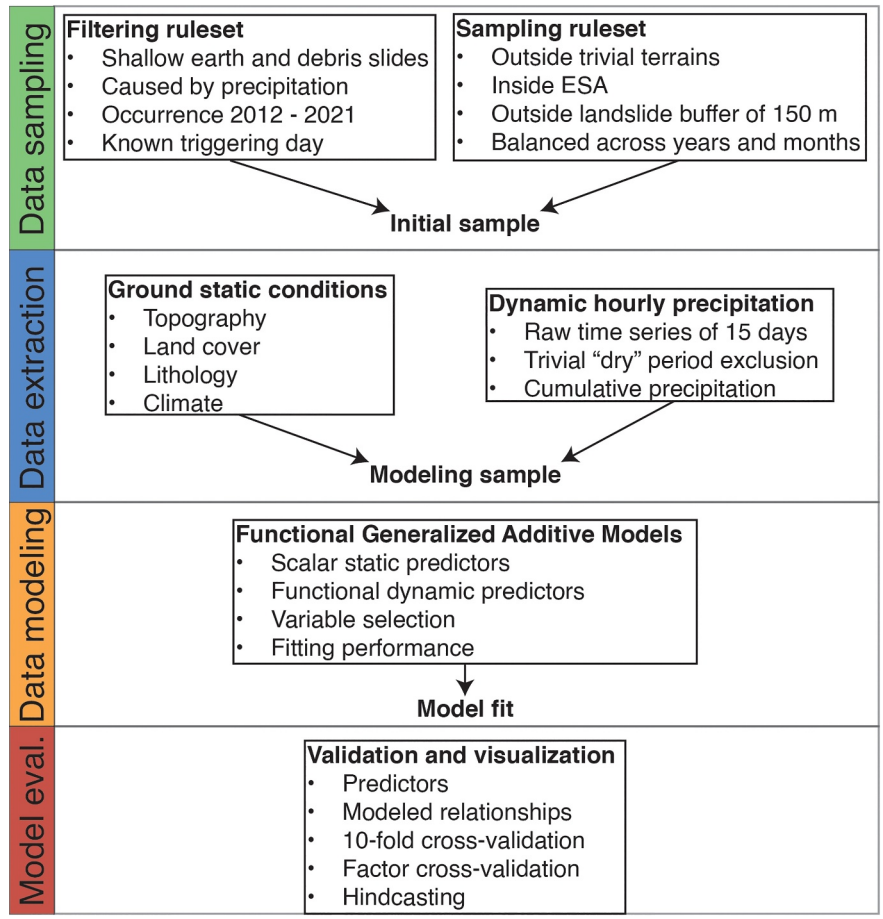

Figure 2. Overview of the implemented methodical approach.

combination of landslide presences and absences in space and time forms the initial model sample, which is subsequently used in the second step, data extraction, to obtain the associated static and dynamic environmental factors. The third step, data modeling, involved data-driven modeling via a binomial functional generalized additive model (FGAM; McLean et al., 2014) to predict landslides using flexible nonlinear predictors based on the temporal patterns observed before their potential occurrence. Model evaluation included analysis of significance (p-values, confidence intervals of predictor curves), plausibility checks, variable importance, multiple cross-validation routines, and a demonstration through hindcasting of a storm event that triggered shallow landslides in the Passeier Valley on 4–5 August 2016.

4.1. Landslide Data Filtering and Absence Sampling

4.1.1. Landslide Presences

The landslide inventory was narrowed down by applying four main criteria: Movement type, material type, cause type, and triggering date availability. Additionally, we performed the analyses on data from March 2012 to December 2021. Although the INCA precipitation data are available since March 2011, the study area was not consistently covered during the first months. Consequently, we opted to restrict the analysis period to begin in March 2012 to ensure consistent data coverage.

4.1.2. Landslide Absences

Ensuring an appropriate selection of landslide absence data is equally critical as selecting the landslide presence data. Notably, sampling landslide absences presents a more complex challenge, as it requires a strategic definition of areas and periods where and when landslides are presumed not to occur. Additionally, because binary

classification models are sensitive to the ratio between landslide presences and absences, systematic biases can be introduced if either presence or absence data are strongly underrepresented or overrepresented (Steger et al., 2017).

We considered two key components to construct the landslide absence sample in space: the ESA mask and the exclusion of trivial terrain. Effectively surveyed areas represent the areas explicitly surveyed while mapping the landslide inventory. We generated the ESA mask to mitigate misleading correlations due to systematic biases arising from the uneven representation of past landslides (Bornaetxea et al., 2018; Moreno et al., 2022; Steger et al., 2021). In other words, this mask restricts the sampling area to ensure that absence observations are only considered within well-observed terrain. The ESA mask is derived from a binary classification model that uses as a target the available landslide data including the events without triggering date. The model incorporates factors such as the proximity to infrastructure (e.g., buildings, roads, railways, pathways) and elevation, generating a spatial prediction that reflects the relative probability of a landslide being recorded based on its proximity to infrastructure and altitude. This procedure to generate the ESA mask has been detailed in Steger et al. (2024). The trivial terrain consists of easy-to-classify areas where no landslides are expected (Steger & Glade, 2017). We identified rocky faces, glaciers, water bodies, and flat lands as trivial terrains to be excluded from the sampling area. The trivial terrains and ESA criteria were equally applied to the landslide presences to keep the sampling strategy consistent. Furthermore, we included a buffer distance around known landslide locations of 150 m as an additional criterion within the filtering ruleset. This ensures that our selected absence samples do not spatially overlap with areas where landslides have previously occurred.

Landslide absence locations were randomly selected within the defined sampling area, with each location being assigned a randomly chosen date between March 2012 and December 2021. The selection was constrained to achieve balanced yearly and monthly distributions to ensure a uniform temporal distribution of landslide absences. This initial data set underwent further filtering by applying a precipitation threshold to exclude "dry" days from the analysis, as detailed in Section 4.2.

4.2. Precipitation Time Series

After obtaining the initial data set comprising the spatiotemporal distribution of landslide presences and absences, we extracted the environmental data. The static or scalar predictors were extracted directly using the sample location and the gridded data sets mentioned in Section 3.2. Additionally, predictors such as the year, month, and day of the year (doy) were derived from the assigned observation dates.

Precipitation data, as the functional predictor, was extracted from the INCA data set for each observation using the sample locations and the assigned observation dates. Following the findings in Moreno et al. (2024), hourly precipitation time series were built up to 15 days prior to the observation dates. Similar to trivial terrains, we defined trivial periods based on a precipitation threshold so that observations with no precipitation amounts $\geq$1 mm on any of the last 72 hr, including the observation day, were excluded from further analysis. This step focuses the problem on predicting precipitation-induced landslides in "wet" conditions and prevents the model from simply learning the difference between "dry" and "wet" conditions. With this procedure, additional landslides not primarily caused by precipitation, such as human interventions, could be excluded. Finally, the precipitation time series were represented in forward cumulative precipitation for each observation, so the last hour at the observation date (day 0–hr 0) contains the total precipitation over the previous 15 days or 360 hr.

4.3. Functional Generalized Additive Models

4.3.1. Theoretical Background

Generalized additive models (GAMs) are flexible statistical approaches that estimate relationships between a response variable and a set of predictors. Unlike traditional models that assume linear associations, GAMs are designed to handle a wide range of error distributions and account for nonlinear associations between the predictors and the response. This is achieved by allowing each predictor to have a smooth function, enabling the model to capture complex underlying patterns flexibly. This adaptability is particularly advantageous when linear functions cannot adequately describe the relationships between predictors and the response (Bolker et al., 2009; Pedersen et al., 2019; Wood, 2017; Zuur et al., 2009).

One of the major strengths of GAMs is their interpretability, especially compared to black-box machine learning models. The smooth functions provide clear insight into the nature of their effects, making it easier to understand how each predictor influences the response. Moreover, GAMs can be extended to model interactions between predictors, providing greater flexibility in modeling complex relationships. Due to their high interpretability and flexibility, GAMs have become widely used across many scientific disciplines, including landslide modeling (Ahmed et al., 2023; Camera et al., 2021; Lin et al., 2021; Lombardo et al., 2020; Moreno et al., 2023). GAMs further allow for probabilistic uncertainty assessment through confidence bounds of the predictions and estimated partial effects of the predictors.

Functional data analysis (FDA) is a statistical framework developed to analyze data recorded as functions over a continuous domain, such as time (Ramsay & Silverman, 2005). In contrast to traditional methods, which focus on scalar observations, FDA considers functions to be the fundamental units of analysis. This approach is particularly useful in settings where the data are expressed as time series with non-negligible temporal correlation or specific temporal patterns that help to improve interpretation and prediction. Various methods have been developed within this broad framework, including functional regression models, where the response or predictors are treated as functional data (Morris, 2015). In this context, scalar-on-function regression is a common approach, where the response variable is scalar, and the predictors are functional, meaning that the predictors are represented as functions rather than a single value.

Building upon these approaches, functional generalized additive models (FGAMs), as presented in McLean et al. (2014), extend the flexibility of GAMs by incorporating the strengths of the FDA. FGAMs allow for the inclusion of both scalar and functional predictors in a single model, making it possible to model the effect of time-varying predictors on a scalar response. Similarly to GAMs, FGAMs facilitate the modeling of complex nonlinear relationships while allowing functional predictors to be treated as smooth curves or surfaces. FGAMs achieve this by decomposing those functional predictors into smooth basis functions, which are then integrated over the functional domain, enabling the model to account for time-varying and time-lagged effects on the response variable. The flexibility and interpretability of FGAMs, inherited from the GAMs, make them particularly valuable in scenarios where temporal dependencies are critical, such as spatiotemporal modeling.

4.3.2. Model Structure and Prediction

The binary indicators of the presence or absence of a landslide event can be coded as

$$Y_i = Y(s_i, t_i) = 1 \text{ if a landslide occurred at location } (s_i, t_i),$$

and $Y_i = 0$ otherwise, with the index $i = 1, \ldots, n$ running through the sample of pixel-hours (with pixel s_i and hour t_i) constructed to include all relevant presences and an appropriately chosen sample of absences, as detailed in Section 4.1. The binary response variable follows a Bernoulli probability distribution,

$$Y_i \sim \text{Bernoulli}(p_i).$$

We apply a logistic link function to relate p_i to the effects of the functional precipitation predictor and the other scalar predictors, be they continuous or categorical. Using the compact notation $P(t) = P(t, s_i)$ for the precipitation series at time t and the location of interest (i.e., at pixel s_i if we predict at (s_i, t_i)), and notation $z_{j,i}$ for the value of other predictors (with indices j) at location (s_i, t_i), the regression equation of the complete model can be generically written as

$$\text{logit}(p_i) = \beta_0 + \sum_{j \in J_1} \beta_j z_{j,i} + \sum_{j \in J_2} f_j(z_{j,i}) + \int_{t_i - \Delta t}^{t_i} f(P(t), t)\, dt.$$

The first sum on the right-hand side gathers all the linear effects of predictors (with indices in a set J_1), whereas the second sum gathers nonlinear smooth functions of other predictors (with indices in a set J_2, usually disjoint from the indices in set J_1), and the final integral term represents the smooth functional predictor of the precipitation series. Specifically, the various functions f are represented as spline functions using spline basis. The

$f(P(t),t)$-term is a tensor product of two univariate spline basis, one for the time dimension and the other for the precipitation intensity. Therefore, we let precipitation interact with time during the time interval of length Δt before the potential landslide event as

$$f(P(t),t) = \sum_{k_1=1}^{K_1} \sum_{k_2=1}^{K_2} \beta_{k_1,k_2} \times s_{1,k_1}(P(t)) \times s_{2,k_2}(t),$$

where β_{k_1,k_2} are coefficients estimated by the model calibration algorithm, and a typical choice for the numbers k_1, k_2 of smooth spline basis functions s_{1,k_1} and s_{2,k_2} in each of the two bases for $P(t)$ and t, respectively, is 10. The integral operator aggregates $f(P(t),t)$ over the time-precipitation field to obtain a scalar contribution to the predictor $\text{logit}(p_i)$. Since there is a large number of coefficients to estimate in the functional term but also in the other smooth terms, a smoothing penalty is applied for each term (i.e., penalizing strong local curvature of the functions f and f_j) with an automatic choice of the smoothing parameters. This avoids overfitting and keeps the model identifiable from data even when the number of the various coefficients $\beta_{\dots}$ is very large and could theoretically even exceed the number of observations. Spline basis functions are by default chosen as thin-plate splines, but we can adapt the choice to specific properties of the data (e.g., cyclic splines to capture the effect of doy that should be periodic since the beginning and end of the year coincide). For more technical details, we refer to specialized literature for generalized additive modeling (Wood, 2017) and extensions to functional regression (Reiss et al., 2017).

Internally, at the beginning of model calibration, the basis function values $s_{1,k_1}(P(t)) \times s_{2,k_2}(t)$ must be calculated for all time steps between $t_i - \Delta t$ and t_i, and for all k_1, k_2. After fitting the model, it can be used to predict the probability p at some new location (s,t) by calculating all relevant predictor components. The number of elementary arithmetic operations is, therefore, much larger for calibration and prediction of FGAM models as compared to classical generalized linear models (without any f-term) or generalized additive models (without the functional term).

Two options are considered and compared for the precipitation series $P(t)$ (where we fix the length of time period Δt preceding a potential landslide event to 15 days, as explained later):

1. Raw precipitation: $P(t)$ is the amount of precipitation observed during one unit of time around t (i.e., 1 hr) at the location of interest.
2. Cumulative precipitation: $P(t)$ aggregates precipitation starting at $t - \Delta t$ at the location of interest, that is,

$$P(t) = \sum_{t_k \in [t-\Delta t, t]} P(t_k).$$

4.3.3. Model Fit

The model fit was performed via the tools implemented in the comprehensive R package refund (version 0.1–37; Goldsmith et al., 2024; McLean et al., 2014). This package allows the fitting of penalized scalar-on-function regression models with structure as presented above, where the scalar binary response is the presence (or absence) of landslides, and the functional predictor is the hourly precipitation time series in a fixed-length segment preceding the time of the observed response.

Models were constructed iteratively by starting with a simple baseline model and manually assessing the relevance of newly added predictors. Predictor assessment was carried out through variable importance analysis and the evaluation of modeled relationships. This assessment was conducted both visually through the investigation of the estimated partial effects and formally through the assessment of p-values, confidence intervals for scalar coefficients, and pointwise confidence envelopes for the various functions $f_{\dots}$. Variable importance analysis gives insights into the relative contribution of each predictor to the response variable. In the FGAM, predictors were ranked based on the estimated proportion of deviance explained, a well-known measure of the goodness of model fit based on the likelihood of the model. We estimated the difference in deviance explained by a full model (i.e., including all the predictors) against a series of reduced models, each omitting a specific predictor. A larger

reduction in deviance explained indicates a greater relative contribution of the corresponding predictor of interest (Goetz et al., 2018). Partial effect plots were used to illustrate how variations in individual predictors influence the estimated landslide probabilities. These plots allow for the interpretation of each predictor effect on the response while keeping all other predictors fixed at their average value, providing a means to assess the plausibility of the modeled relationships. For the case of the functional predictor, the partial effect plots were visualized as contour plots to represent the nonlinear interactions between precipitation time series, time, and the response variable.

4.4. Model Validation and Visualization

For model evaluation, especially predictive performance, we employed a set of well-established diagnostic tools. The model performance was assessed using the R package sperrorest (version 3.0.5; Brenning et al., 2022) through several approaches: k-fold random cross-validation (RCV), k-fold spatial cross-validation (SCV), temporal cross-validation (TCV) based on both years and months, and leave-one-factor-out cross-validation (FCV) using lithology.

Random cross-validation involves repeatedly partitioning the available data set into disjoint training and testing sets, in our case, using 10 folds and 10 repetitions, resulting in 100 iterations (Brenning, 2012). The area under the Receiving Operator Characteristics curve (AUROC) was computed for the independent testing sets to assess the predictive performance for each partition. The ROC curve graphically represents the performance of a binary classifier by varying the discrimination threshold. At the same time, the AUROC value usually ranges from 0.5 (i.e., random classification) to 1 (i.e., perfect discrimination), with higher values indicating a better-performing model (Hosmer et al., 2013). Conventional RCV routines may fail to capture the spatial variability of the model performance, potentially leading to over-optimistic results if the spatial model predictions poorly align the data within a specific subregion of the study site. Thus, we applied SCV, which can be used to estimate the spatial transferability of the model and reveal spatially incoherent predictions. This study's underlying spatial partitioning approach was achieved through a k-means clustering approach, with 10 folds and 10 repetitions, mirroring the RCV setup.

We also applied TCV and FCV to assess model transferability across time and lithological units in addition to the cross-validation routines described earlier. Temporal cross-validation was performed by iteratively excluding observations from either 1 month (leave-1-month-out) or 1 year (leave-1-year-out) from the training data set. This was followed by evaluating the model predictions on the excluded data using the AUROC. Similarly, FCV was applied using the five different lithological units to define the training and testing data sets.

For visualization purposes, we used our dynamic model in a demonstration test. Ideally, the model can simulate any day of the year, given the availability of precipitation data prior to that day. To illustrate its practical application, we conducted a hindcast for the landslides triggered by the storm event on 4–5 August 2016 in the Passeier Valley using the precipitation time series for those respective dates. The estimated model predictions were then compared to the landslide inventory mapped by de Vugt et al. (2024), which documented the same storm event.

5. Results

5.1. Landslide Data Sampling

After applying the first filtering ruleset, the initial 11,944 landslide observations in the IFFI data set were narrowed down to 335 shallow earth and debris slides caused by short-intense and prolonged precipitation with a known triggering day between March 2012 and December 2021. This subset was refined by excluding observations located within trivial terrain and outside the ESA, resulting in 307 landslide records. Specifically, we excluded 15 landslides outside the ESA mask and 13 on trivial terrain. Similarly, a precipitation threshold was applied to exclude trivial periods, retaining only observations with precipitation exceeding 1 mm during the 72 hr preceding the landslide date. We obtained a final sample size of 259 landslide observations following this final filter.

The combination of the landslide presence and absence samples resulted in a total of 6,448 observations (Figure 3a), with 6,138 corresponding to landslide absences, yielding a ratio of approximately 1:20 in terms of landslide presence and absence, respectively. The temporal distribution of absences was kept uniform across years and months. In particular, the initial monthly absence sample was proportional to the number of days each

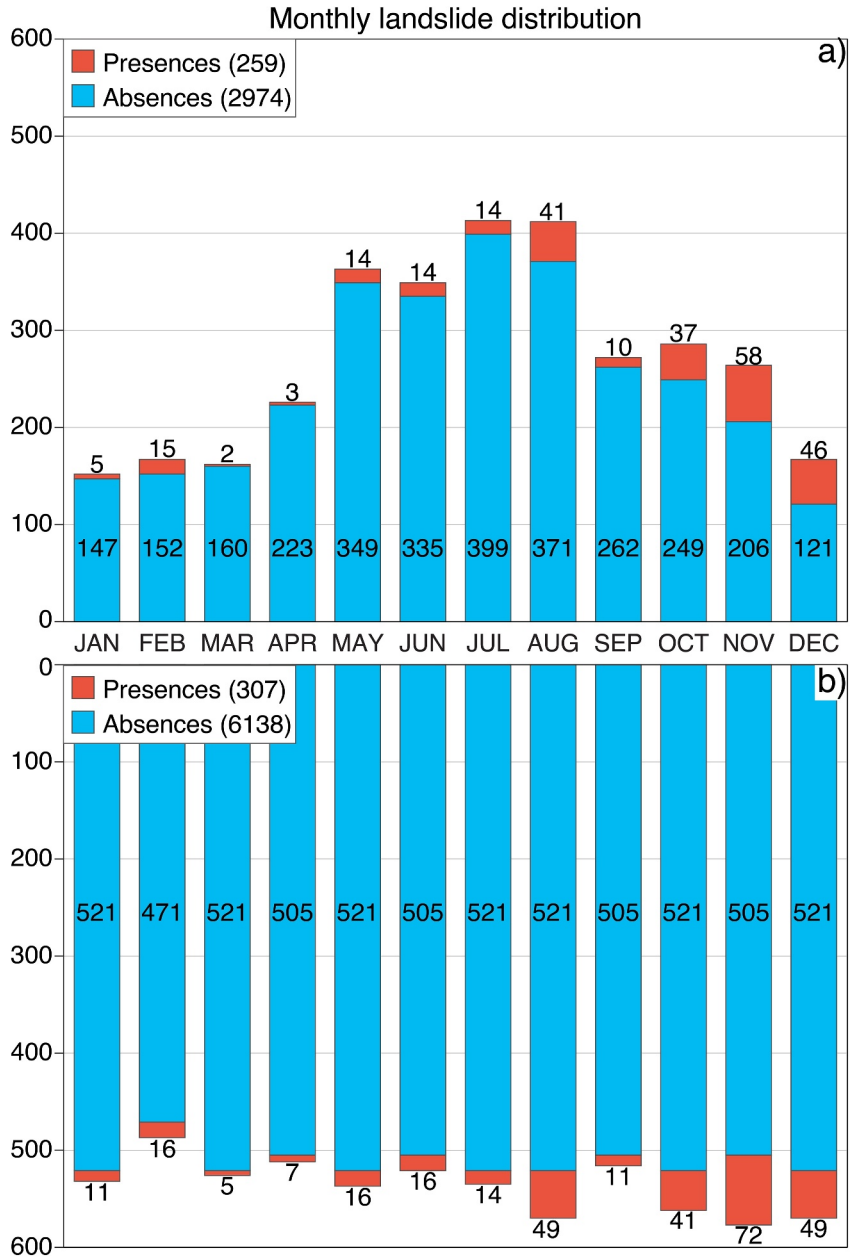

Figure 3. Data sampling results. The bar plots show the monthly frequency of the sampled data before (b) and after (a), excluding the trivial periods. Landslide presences are colored red, while the absences are in blue.

month. After using the precipitation threshold to exclude the trivial periods, we obtained a final modeling sample that only included the days with precipitation exceeding 1 mm during the last 72 hr before the observation day, resulting in a total of 3,233 observations. This final sample comprised 259 landslides and 2,974 absence samples, representing a ∼50% reduction from the initial data set and an updated presence-to-absence ratio of about 1:10. Notably, 48 landslide observations were potentially removed because they were not primarily caused by precipitation. Since we completely removed non-ESA locations and times with preceding negligible precipitation activity from the data set, the relative landslide occurrence probabilities estimated by the model we implement must be interpreted conditionally to be within the ESA region and the presence of preceding precipitation. Achieving good predictive scores of the model is more challenging in this setting since trivial conditions are removed. On the other hand, it is also facilitated since some noisy observations, that is, landslides occurring in trivial conditions with triggers other than precipitation, are also excluded.

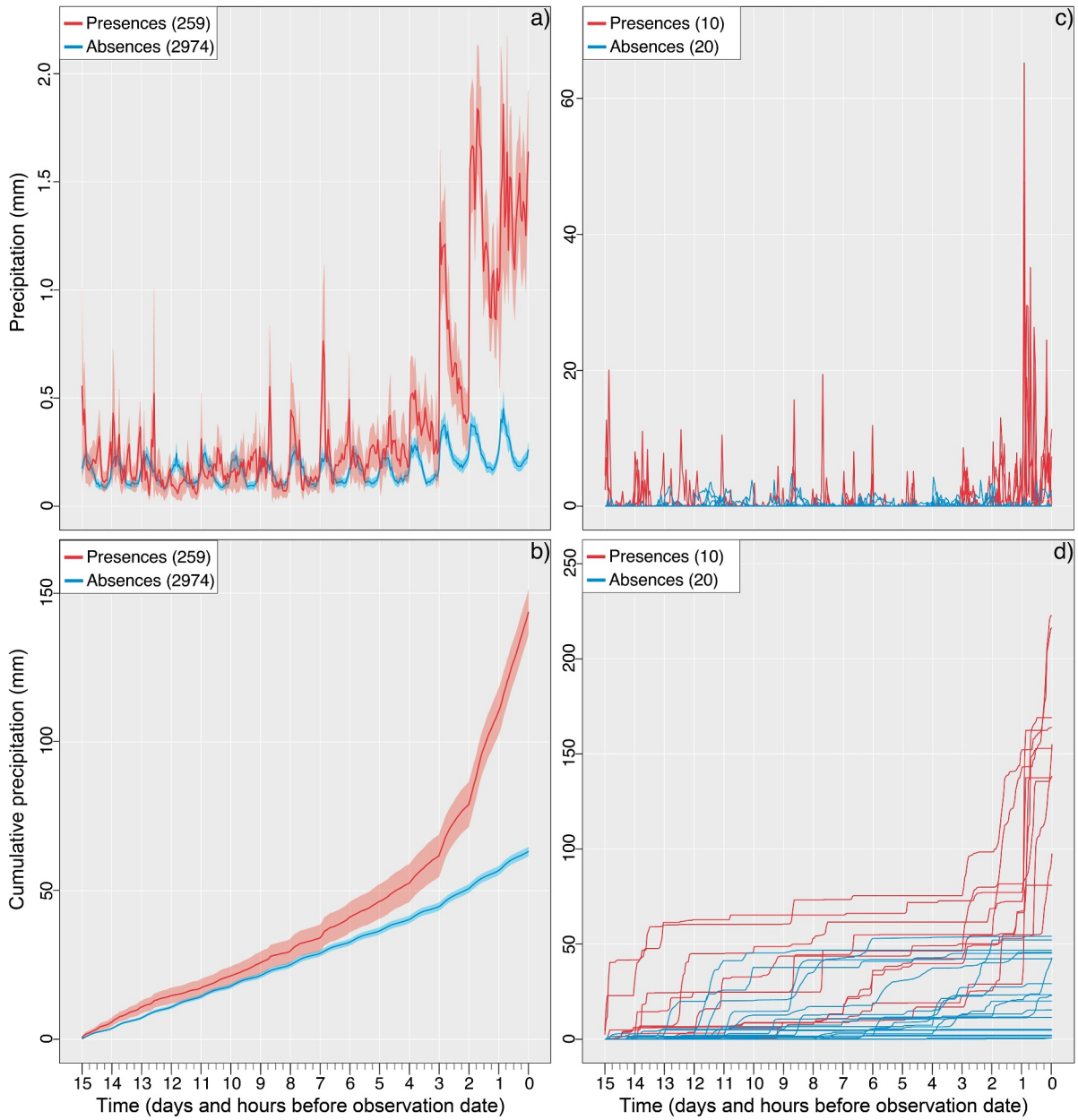

Figure 4. Precipitation time series extraction. The plots show the average hourly time series of precipitation (a) and cumulative precipitation (b) in solid lines, with the 95% confidence interval in dotted lines for landslide presences (in red) and landslide absences (in blue) up to 15 days before the observation date. Panel (c) shows examples of the hourly time series of precipitation and (d) cumulative precipitation for 10 randomly selected presence and 20 absence samples.

Figure 3b shows that observations with precipitation were relatively more frequent during summer months (i.e., May, June, July, and August). Interestingly, although November had fewer "wet" days, it exhibited the highest frequency of landslides. This suggests a seasonal influence consistent with the findings in Steger et al. (2023), where it was noted that a rarer precipitation day in November is more likely to be associated with landslide occurrence than an average precipitation day during the summer.

5.2. Precipitation Time Series

Based on the previously constructed data set, we extracted static geo-environmental factors and precipitation time series data. After applying the precipitation threshold, Figure 4a shows the average precipitation across hours and the corresponding 95% confidence interval for landslide presences (in red) and absence samples (in blue) for the

Table 1
Model Setup

Predictor	Deviance explained	Smooth function	Significance (p-value)	
Cumulative precipitation time series	0.282	Tensor product	<0.001	
Slope	0.065	Thin plate spline	<0.001	
Standard height	0.029	Thin plate spline	<0.001	
Forest	0.013	Factor term	No	Ref. Level
			Yes	<0.001
Mean precipitation	0.012	Thin plate spline	0.002	
Lithology	0.006	Factor term	Crystalline	Ref. Level
			Porphyry	0.239
			Sedimentary	0.084
			Plutonic	0.508
			Calcschist	0.033
Doy	0.003	Cyclic cubic spline	0.063	

Note. Predictors introduced in the binomial FGAM and their variable importance. The tensor product smooth function of the cumulative precipitation series captures the interaction of hourly time lag and precipitation (with thin plate spline bases for each of these two dimensions), contributing to possible landslide occurrence.

3,233 observations. Overall, landslide presence samples experienced, on average, higher hourly precipitation than absence samples over the 15-day analysis period. The differences became particularly pronounced between days 0 and 5, with landslide samples typically showing time stamps with approximately 1.5 mm more precipitation on average than absence samples.

The analysis using cumulative precipitation for each event in Figure 4b further highlighted these differences, with up to 100 mm more precipitation observed for landslide presences than absence observations during days 0–5. Given the smoother and more stable nature of the cumulative precipitation signal, as opposed to the more erratic fluctuations of hourly precipitation, we opted to use cumulative precipitation data from day 0 up to day 5 for the subsequent modeling procedures. These differences are highlighted during the discussion in Section 6.

5.3. Model Fit and Model Relationships

We performed the model fit iteratively by starting from a model with only an intercept and then incorporating other components one by one to analyze their added value for explanation and prediction. The non-reported iterations were evaluated regarding the significance of the predictors (p-values of components and goodness-of-fit criteria such as AIC) but also the plausibility of the partial effect plots (through visual inspection), leading to the final model fit, as summarized in Table 1, along with other details on the FGAM parametrization. After the final model had been established, the relative contribution of each predictor was determined through variable importance analysis based on the statistical notion of deviance, with a higher proportion of deviance explained, indicating a higher contribution to the model. All the selected predictors increased the deviance explained by the model, with the precipitation time series (0.282) emerging as the most important factor in predicting landslide occurrence. The topographic predictors, such as the slope steepness (0.065) and the standardized height (0.029), also showed relevant contributions. In contrast, the lithology (0.006) and the doy (0.003) had much less influence on the occurrence of landslides.

The partial effect plots provided a clear summary of the modeled relationships. Figure 5a illustrates that the estimated regression coefficients (RC) generally increase as cumulative precipitation rises and time progresses, peaking on the final observation day for cumulative precipitation amounts exceeding 100 mm.

Figures 5b–5e depict how estimated landslide probabilities vary with changes in mean annual precipitation, doy, slope steepness, standard height, forest, and lithology. For instance, mean annual precipitation indicates higher landslide probabilities in relatively drier areas (600–900 mm), whereas wetter regions (1,100–1,400 mm) show low probabilities. Regarding doy, the analysis reveals slightly reduced probabilities around doy_{200}, corresponding to mid-July, the summer season. However, the significance of the effect is not clear, as can be seen in the p-value

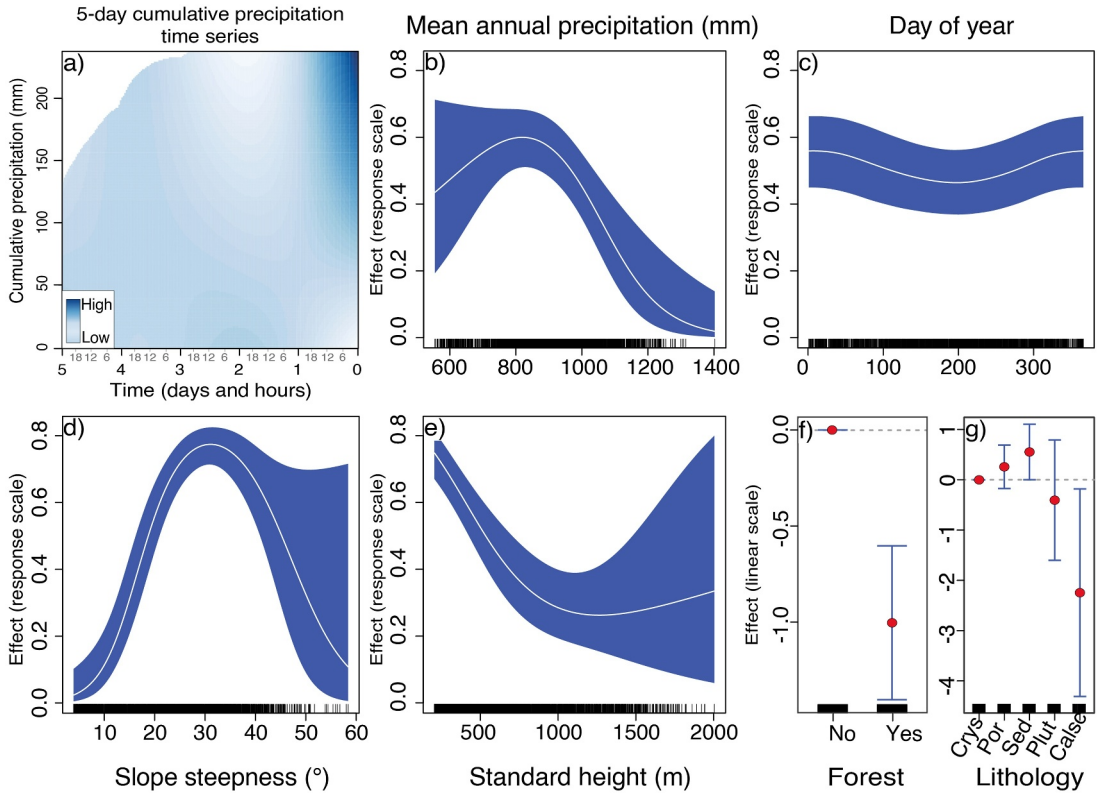

Figure 5. Partial effect plots. Panel (a) shows the interaction effect of the cumulative precipitation time series and time, with the *y*-axis expressing the cumulative precipitation, the *x*-axis representing the time in days and hours, and the colors representing the regression function (darker color for higher values). In panels (b–e), the center lines in white show the mean estimated effect, and the blue bands show the associated 95% confidence interval, with the *y*-axis expressed at the response scale. Panels (f, g) show the mean estimated effect (red dots) with the associated 95% confidence interval with the *y*-axis expressed at the linear scale.

from Table 1 and the fact that the confidence bounds are relatively wide (Figure 5c). Topographic predictors, such as slope steepness, exhibit a parabolic trend with lower landslide probabilities at 0° inclination, reaching its maximum at ∼30° and diminishing for slopes up to ∼60°. In the case of the standard height, the landslide probabilities show a nonlinear trend, with probabilities gradually decreasing as the height values increase.

Categorical predictors presented in Figures 5f and 5g included the land cover and lithology. The different land cover classes were iteratively tested, and the class that showed plausible and statistically significant results was simplified to a binary predictor: the presence or absence of forest. These results show that the forest presence negatively influences the occurrence of landslides. For lithology, the classes that showed statistical significance (with reference to class crystalline) were sedimentary and calschist, with sedimentary rocks associated with positive RC and calschist with negative coefficients.

5.4. Model Evaluation and Visualization

The cross-validation routines outlined in Figure 6 demonstrate a high model generalization and transferability, with AUROC scores consistently exceeding 0.90, indicating outstanding discrimination as defined by Hosmer et al. (2013). The two 10-fold cross-validation strategies (Figure 6a) RCV and SCV yield median AUROC values of 0.929 and 0.927, respectively. As expected, SCV using k-means clustering shows slightly lower performance with a wider interquartile range (IQR) compared to RCV, as SCV reduces residual dependence from the spatial data set, providing a less biased evaluation of the predictive capability.

Leave-one-out cross-validation routines, such as TCV (for years and months) and FCV (for lithology) in Figures 6b–6d, show mean AUROC values of 0.881, 0.885, and 0.937, respectively. Lower performance scores in specific years, months, and lithological units likely reflect variations between the conditions driving landslide occurrences in these units and those captured in the model, which was trained on the remaining units. Temporal

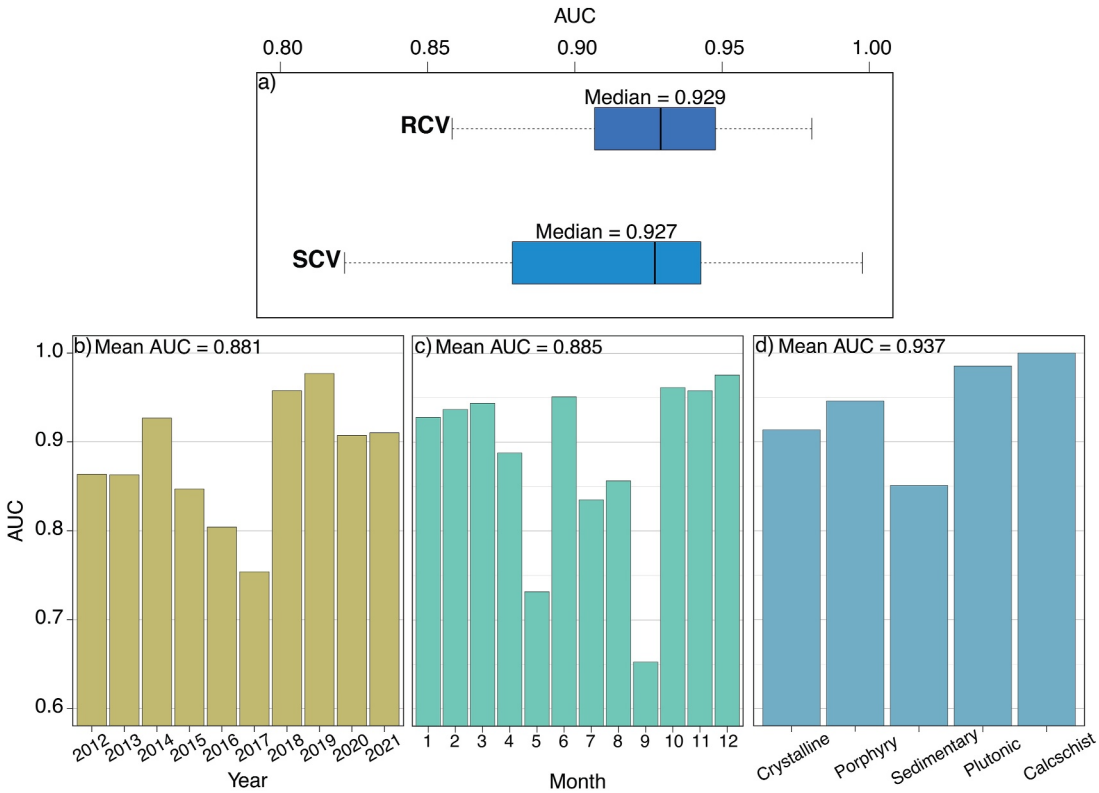

Figure 6. Summary of the model performance. Panel a shows the 10-fold random cross-validation and 10-fold spatial cross-validation, whereas the remaining panels show the temporal cross-validation for years and months and FCV for the lithological classes.

cross-validation for years and months demonstrates robust temporal transferability, with performance scores slightly lower for 2017 and 2016 and higher for 2019, 2018, and 2015. At the monthly level, lower performance scores are observed in May and September, likely due to abrupt changes in precipitation patterns: an increase during the transition from April to May and a decrease during the transition from September to October (Crespi et al., 2021). In contrast, the period from October to March shows the highest AUROC values. On the other hand, FCV reveals AUROC values above 0.9 for all lithological classes except sedimentary, which scores ~0.85. This indicates that the modeled relationships are generally well transferred across the lithological units with lower performance for the sedimentary units.

For visualization purposes and to demonstrate the predictive capabilities of the model, we applied the model to hindcast the landslides triggered during a storm event that took place in the Passeier Valley on 4–5 August 2016. This localized storm event was characterized by strong precipitation that triggered numerous landslides in the catchment of the Passeier River, making it a suitable case study to evaluate its predictive capabilities. The resulting predictions are stored as the animation GIF file, Movie S1, and provided in Supporting Information S1.

Furthermore, Figure 7 displays a selection of four specific frames from this animation file, focusing on the critical period from 03:00 to 21:00 on 5 August. These frames illustrate both the hourly precipitation data, sourced from the INCA data set, alongside the corresponding landslide probabilities generated by the model. Examining these frames makes it possible to observe how the landslide probabilities evolve dynamically in response to increasing precipitation over time. At the onset of the selected time interval (03:00), when the precipitation peaks, the model predicts relatively low landslide probabilities across the affected area. However, as time progresses and the cumulative impact of precipitation becomes more pronounced, the predicted landslide probabilities increase. By 15:00, the model indicates moderate landslide probabilities, particularly near the main valley bottom, which subsequently peaked at 21:00, revealing high landslide probabilities in the area of interest.

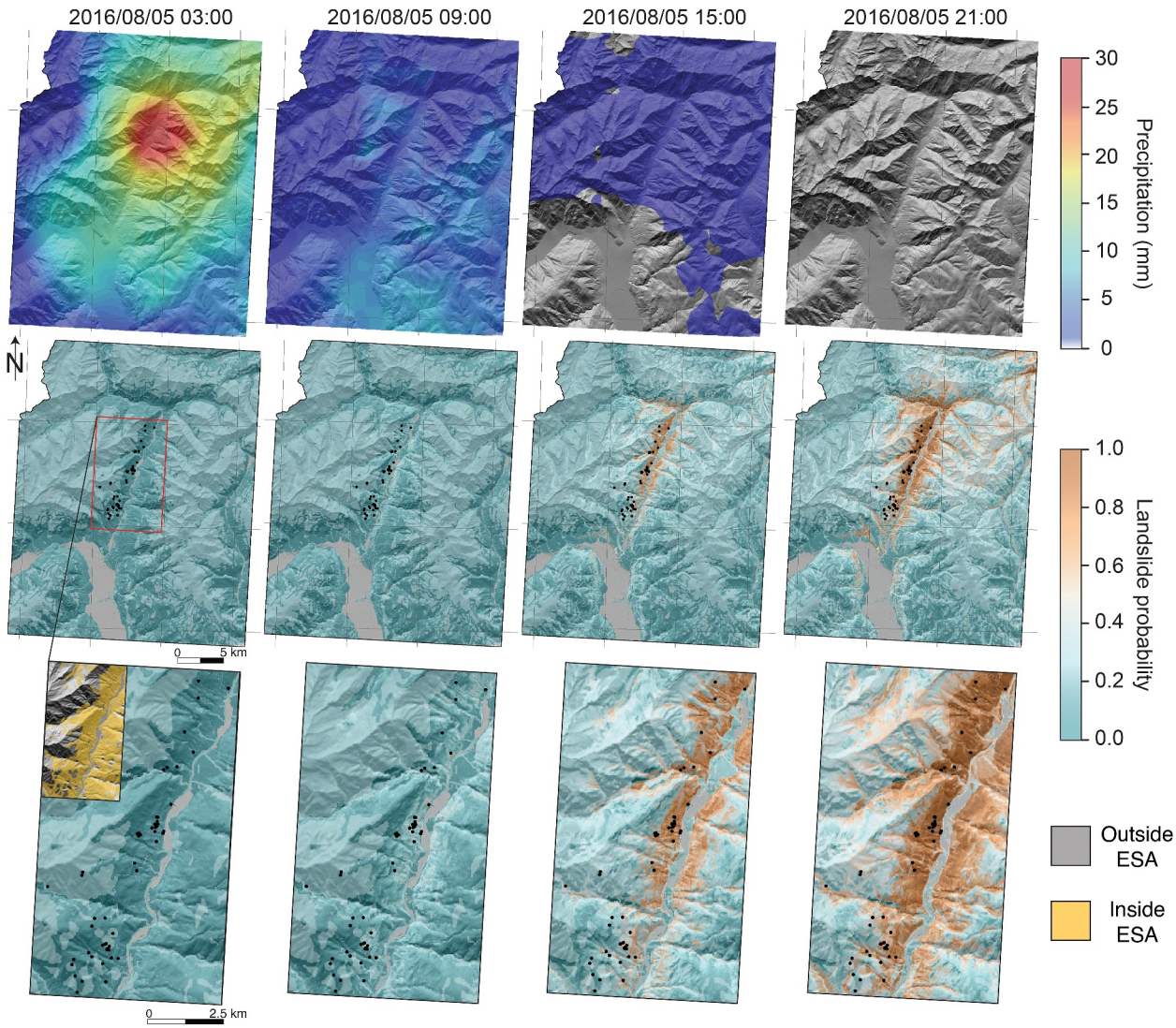

Figure 7. Extract of the dynamic landslide predictions for hindcast on landslides associated with the precipitation event in the Passeier Valley on 4–5 August 2016. The first row shows the precipitation amounts on 5 August from 03:00 UTC to 21:00 UTC, whereas the second row shows the associated landslide predictions, highlighting the areas within the ESA mask in darker colors. The last row is a zoom to visualize better the independent landslide inventory mapped in de Vugt et al. (2024) as points colored in black and the areas within the ESA mask in yellow (most minor panel).

6. Discussion

In this study, we implemented a space-time classification framework that integrates static scalar and dynamic functional factors to predict the occurrence of precipitation-induced shallow landslides. The proposed model exhibits high predictive performance, regularly achieving AUROC scores surpassing 0.90. This indicates the ability of the model to account for various influencing factors, including static ground conditions, precipitation as a function of time, seasonal effects, and spatial biases. The discussion below covers the key aspects of this research, focusing on the sampling strategy, the considerations from a mechanistic viewpoint, and the potential for early warning applications.

6.1. Considerations on Sampling Strategy

Most current space-time models treat space continuously, while time has mostly been treated discretely, either according to event-based inventories or aggregated over extended periods such as years or seasons (Ahmed et al., 2023; Dahal et al., 2024a, 2024b; Wang et al., 2022). In contrast, our model preserves time in its original

continuous daily resolution for landslides and hourly for precipitation, a strategy that inevitably leads to several orders of magnitude larger numbers of landslide absences as opposed to the presences. Modeling such a daily spatiotemporal domain is impractical, computationally highly demanding, and technically, it would require slightly different formulations compared to standard models. In fact, the use of binomial models would need to be extended to a framework typical of zero-inflated regressions (Lambert, 1992). Therefore, to bypass all these limitations, we devised a sampling design to uniformly capture spatiotemporal variability of presence-absence conditions, keeping the sample to a reasonable size while excluding trivial and potentially biasing information from the data. This approach, as presented in Steger et al. (2024), involved applying several key rules, namely: (a) Masking out trivial terrains (Steger & Glade, 2017), (b) sampling exclusively within the effectively surveyed area (Bornaetxea et al., 2018), (c) excluding samples within a 150 m radius of each landslide location, (d) balancing absence samples across years and months, and (e) masking out trivial time periods (Moreno et al., 2024). We recommend analogous considerations and present the current protocol as a blueprint for future studies with similar space-time data structures.

We acknowledge that 13 landslides were excluded from further analyses due to masking out trivial terrains, even though, in theory, no landslides should occur in such areas. Several reasons may explain this mismatch, including the input data uncertainty and temporal variations in land cover. However, before addressing these potential sources of error, it is necessary to clarify what the trivial terrain mask represents. Trivial terrains constitute a mask derived from topography and land cover. The former corresponds to flatlands (derived based on a slope steepness threshold), whereas the latter encompasses glaciers, rocky faces, and water bodies. Here, we assumed that topography remained unchanged over time. However, land cover is dynamic and subject to intra- and interannual variations—for instance, glaciers retreat, and water bodies fluctuate. The trivial terrains were extracted from a 2015 land cover map and assumed to remain static throughout our period of interest. This consideration, along with the inherent uncertainty in the input data used to delineate the estimation of trivial terrains, may have led to the exclusion of 13 landslides from the initial subset. Despite this limitation, we consider the mask filter a necessary step to ensure consistency in our sampling strategy, maintain plausible modeled relationships, and prevent the artificial boost in the predictive performance due to the inclusion of easily classifiable areas. While this approach comes at the cost of losing some presence samples, it ultimately strengthens the reliability of our model.

The concept of easily classifiable areas constitutes a crucial element of discussion, and for clarity, we elaborate on it further here. Including trivial areas in the modeling process would lead any flexible model to set drastic changes in RC in steepness values near zero, followed by a sharp increase for values exceeding this threshold (Felsberg et al., 2022; Steger & Glade, 2017). However, neither the scientific community nor stakeholders are interested in developing models that simply discriminate susceptible slopes between flat and steep ones. This is indeed a trivial notion, which is why we excluded easily classifiable terrains to force our model to discriminate susceptible conditions within actual steep terrains. Any model should do this, hence, our choice to spatially constrain the modeling procedure.

The concept of triviality takes on a different meaning when considered from a temporal perspective. In this study, we applied a precipitation threshold to filter out observations that received less than 1 mm of precipitation in the 72 hr before the day of observation. This resulted in excluding 48 landslide presences (∼15% of the original subset) and 3,164 absence samples (∼50% of the original subset). This step was necessary because, without it—and given that our focus is on precipitation-induced shallow landslides—the model would primarily differentiate between "dry" and "wet" conditions rather than making a distinction between landslide occurrence in "wet" conditions and non-landslide occurrence during similar conditions. We acknowledge that the exclusion of the landslide observations is not ideal and may stem from several factors, including (a) errors and uncertainty in the available precipitation data, (b) landslide times wrongly reported as well as their causes, and (c) the choice of precipitation threshold. The selection of this threshold involves a trade-off: a longer time window could exclude fewer presence instances but would simultaneously increase the number of absence samples. This could potentially bias the model by wrongly representing seasonal precipitation patterns in the study area. Conversely, shorter time windows, such as the 2 days applied in Steger et al. (2023) and Moreno et al. (2024), would have led to the removal of a substantial portion of both presence and absence samples. Through extensive unreported testing, we found 72 hr to provide a reasonable trade-off. Such a compromise retains sufficient presence samples and maintains a balanced absence data set where the seasonal patterns are still preserved (as shown in Figure 3).

Analogously to the discussion on easily classifiable areas, we further detail the concept of easily classifiable times. Including trivial times in the modeling process would lead any flexible model to set drastic changes in RC near zero precipitation, followed by a sharp increase for values exceeding this threshold. However, neither the scientific community nor stakeholders are interested in developing models that simply discriminate susceptible slopes subjected to precipitation or no-precipitation conditions. This is why we excluded easily classifiable times to force our model to discriminate susceptible conditions during "wet" periods. Any model should do this, hence, our choice to temporally constrain the modeling procedure.

6.2. Considerations From a Mechanistic Viewpoint

Beyond performance-oriented considerations, models that treat precipitation as a continuous signal offer the inherent advantage of bypassing the need for arbitrary aggregation choices over time. In other words, no expert choice is needed; rather, the data-driven tool of choice is already tasked with finding the best functional relations. Conversely, space-time solutions treating precipitation as a scalar predictor require a preprocessing step where the model iteratively evaluates various time windows to determine the most suitable representation (Gómez et al., 2023; Moreno et al., 2024; Nocentini et al., 2023; Smith et al., 2023). Another key feature of our model is its ability to inherently use the entire time series to estimate and account for lagged precipitation effects. This allows the model to incorporate delayed responses in its predictions. As shown in Figure 7, and the supplementary animation Movie S1, the model reveals how the initial precipitation amounts do not immediately produce an equivalent increase in the dynamic landslide probabilities. Instead, this increase occurs much later in the simulation when the lagged precipitation contributions become relevant and added to subsequent precipitation.

We stress this to be particularly valuable information. From a fundamental geomorphological perspective, shallow landslides typically respond to precipitation with a relatively short delay between the incoming precipitation and their potential failure (Crosta & Frattini, 2003). In contrast, deep-seated landslides operate on a different time scale, requiring longer lag times due to the prolonged percolation before the water reaches and lubricates the sliding surface (Kuo et al., 2021).

The value of this information lies in its native estimation as part of our FGAM procedure. To put things in perspective, rigorous lag time estimations are achievable at the slope scale through geotechnical models. However, such models require soil and sock physical properties, expressed at least in terms of permeability values associated with the given medium. At regional scales, obtaining an adequate geotechnical description of a given landscape is challenging—if not infeasible—due to the extensive financial, time, and personnel investments. Therefore, a physically quantifiable lag time is equally not feasible unless considerable simplifications are implemented. Our model inherently represents precipitation as a continuous function, thus capturing the required delay between the onset of precipitation and the increase in landslide occurrence probabilities. In this sense, this indicates the lag time, which future research could explore further by modeling different landslide types. For instance, one could estimate the time gap between the start of the precipitation time series and the peak susceptibility for debris flow and debris slides, and their translational and rotational expression. It is important to stress that if it is true that our model returns an apparent lag time, it is important to note that this estimation lacks a direct physical interpretation. We do not have enough information to support a mechanistic interpretation of such values. Therefore, a possible venue for future research could include comparing data-driven lag times against physics-based ones.

Beyond interpreting the term on the precipitation time series, our FGAM allows for the same capabilities for any other predictor (e.g., temperature, deformation, snow cover, soil moisture). Particularly, variable importance assessment and the partial effect plots provided valuable insights into the statistical contributions of both scalar static and functional dynamic predictors to landslide occurrence across space and time. Consistent with classification standards in Hosmer et al. (2013), the model shows outstanding discrimination capabilities, supported by multiple implemented cross-validation routines across space, time, and environmental factors. However, this predictive performance is achieved by combining predictors whose interpretation is not always straightforward. This dual nature—an advantage and a limitation—is characteristic of data-driven models, which often rely on proxy variables instead of actual physical quantities. For instance, including doy as part of our predictor set serves as a proxy for seasonal effects. However, it does not explicitly account for the effects of antecedent precipitation or soil moisture conditions preceding the slope failure (Monsieurs et al., 2019). For shallow landslides, antecedent soil moisture is critical in regulating rainwater infiltration and ultimately triggering slope failure (Greco

et al., 2023). While our model incorporates hourly precipitation time series spanning 5 days alongside doy, it does not fully capture these complex hydrological dynamics. We therefore recommend that future studies explore the inclusion of antecedent soil moisture in such a modeling framework (Thomas et al., 2019; Wicki et al., 2020).

Another important aspect of seasonality is the higher occurrence of landslides during the late autumn and early winter months (October, November, and December) despite fewer "wet" days (Figure 3). While our sampling strategy captures this pattern, and our model incorporates predictors such as the precipitation time series and the doy, we acknowledge that it may not fully account for these complexities. As mentioned earlier, the key factor is not just precipitation but also the amount of water ultimately infiltrating and contributing to pore pressure increases. During these months, lower temperatures and potentially reduced rates of evaporation, interception, transpiration, and plant water absorption likely result in more water remaining in the soil, even when precipitation is less frequent (Molnar & Burlando, 2008; Norris et al., 2008; Schmaltz et al., 2019). To better capture this effect, we again recommend further research exploring the inclusion of antecedent soil moisture (Peiro et al., 2024; Stanley et al., 2021), evapotranspiration proxies, or net recharge estimates.

6.3. Considerations on Model Potential for Early Warning

We believe that the model holds the potential for advancing LEWS. However, we also recognize that it is currently far from being ready for operational purposes. This is mainly because calculating the functional predictor is inherently time-consuming due to the large number of elementary arithmetic operations required. Such an intensive task was conducted on the ITC geospatial computing platform (CRIB; https://crib.utwente.nl/; Girgin, 2021) using a computing setup equipped with 72 vCPUs (Intel x86–64), 768 GB of RAM, and an NVIDIA RTX A4000 GPU. This limitation poses a critical barrier, as deploying an effective EWS requires seamless nowcasting and forecasting of landslide occurrence probabilities. Under the current setup, several data conversions and I/O operations are required, resulting in a rather lengthy and slow process. Beyond computational considerations, we acknowledge challenges in applying this framework for forecasting purposes since the forecasted precipitation amounts would need to be elaborated further into time series to enable landslide predictions. While it is acceptable and manageable for research, new and more flexible computational strategies are essential to meet the demands of real-time operational systems.

A critical point for consideration—and one that may invite critique—concerns benchmarking our results against a space-time model designed according to the standards for EWS. Traditional EWS relies solely on precipitation information, thus leaving aside the contribution to the prediction brought by landscape characteristics. Moreover, the use of the precipitation signal itself is aggregated to a scalar value for a specific time window of interest by computing the precipitation sum. To illustrate this comparison, we created Figure 8, where Figure 8a displays the model performance only using precipitation in its raw (blue) and cumulative (red) forms. As for Figure 8b, we reported the performance of an equivalent model to which landscape characteristics such as slope steepness, lithology, standard height, land cover, mean annual precipitation, and doy have been incorporated. Ultimately, Figure 8c depicts the performance obtained using a functional representation of the precipitation together with landscape-related predictors.

What stands out is that the use of raw precipitation—the precipitation amounts before computing the cumulative values—is consistently the wrong choice when the signal is aggregated per fixed time windows (the blue line is the lowest across the three panels). The same cannot be said for our functional approach, where the distinction between raw and cumulative precipitation as continuous signals leads to essentially very similar results (blue and red lines in panel c). As for the use of aggregated precipitation, interestingly, even Figure 8a shows remarkable prediction capabilities when it comes to cumulative precipitation (red line in the left panel), although it still underperforms compared to the models in Figures 8b and 8c. When focusing on the latter panels, we observe that our functional approach is slightly better, irrespective of how one processes the precipitation signal (red or blue lines). Overall, scalar and functional cumulative precipitation lead to negligible variations between Figures 8b and 8ure 8c that need to be acknowledged. This implies that a scalar use of the precipitation signal, if it is combined with landscape properties, leads to very satisfying results. An important difference is highlighted in work carried out by Fang et al. (2023), where there was an improvement in predictive power of ∼20% between a model treating precipitation functionally or in scalar form without the support of terrain attributes. Similarly, the functional treatment of the precipitation signal in Lim et al. (2024) brought a ∼10% improvement with respect to a scalar baseline in a model equipped with terrain properties in both cases. Irrespective of the prediction gain, a key

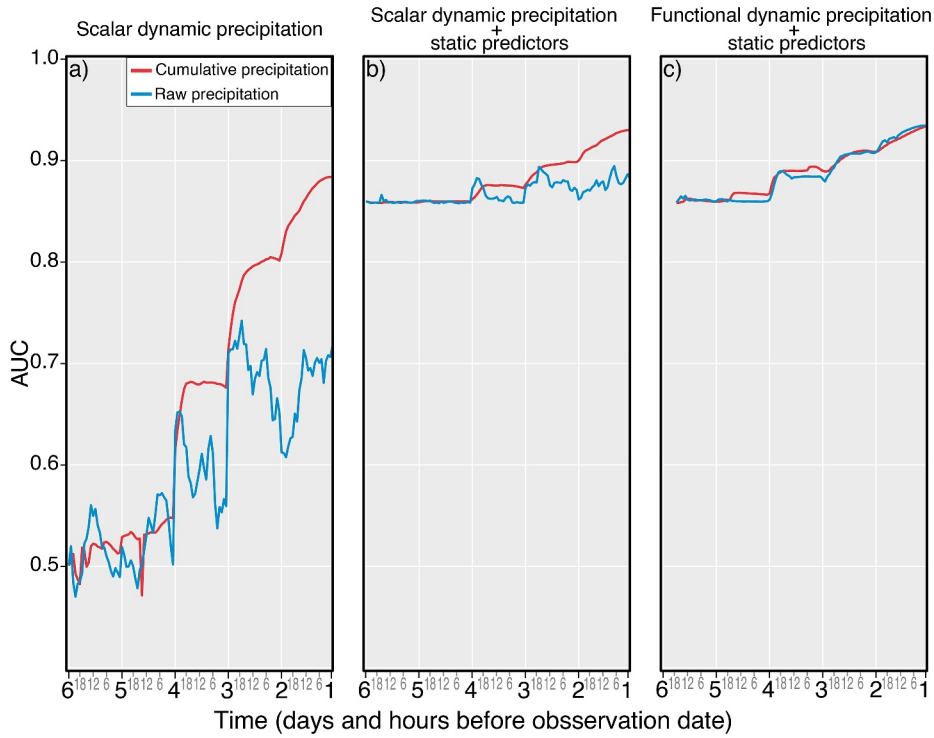

Figure 8. Illustration of the benchmark performance report. On the *x*-axis are the time intervals (in hours and days) for which precipitation was considered in the models, whereas the *y*-axis indicates the corresponding AUC scores. In each panel, blue lines represent models that use raw precipitation, and red lines represent models that use cumulative precipitation. Panel (a) displays models using solely scalar precipitation predictors; panel (b) incorporates both scalar precipitation predictors and landscape characteristics; and panel (c) integrates the landscape characteristics with the precipitation in its functional representation. Note that the cumulative precipitation was computed forward in time, meaning that T_{d1h0} (day 1 at hr 0) reflects the total precipitation over the entire period of analysis. For panel (c), the time series begins 6 hr into the period (T_{d6h18}) and progressively extends at each subsequent timestamp until the entire time series is incorporated at T_{d1h0}.

advantage of the functional model is its ability to leverage the entire time series, eliminating the need for cumbersome tests across various time windows—a process typical of EWS setups. This efficiency favors functional models for practical implementations, a tradeoff with computational needs.

7. Conclusion

Throughout the experiments conducted in this research, several noteworthy findings emerged, particularly in comparison to standard early warning practices. A functional representation of precipitation captures lagged effects, a feature yet to be observed in the landslide early warning literature, a field of research where we will further place future efforts. Another important element is the contribution of the landscape characteristics in addition to the dynamic contribution of precipitation. Current technological advancements have made it difficult to justify using a model that relies solely on precipitation for threshold estimation and a separate model based on terrain characteristics for susceptibility estimation. Data-driven models have already achieved a degree of flexibility, and computational environments now offer sufficient resources that allow the integration of static and dynamic predictors in a single tool. This shift could lead to a fundamental change in focus from precipitation thresholds to unified landslide probability thresholds if widely accepted. We expect this will be the direction the geoscientific community will take in the coming years, with our work contributing to this potential evolution.

A functional representation of the precipitation certainly removes the need to identify the best time windows for aggregating precipitation. Still, more could be done regarding how one considers the precipitation signal. We are currently testing our functional approach with precipitation signals interpolated from rain gauge records, terrestrial radar stations, and satellite products. This is an area where we expect further differences between a functional and a scalar precipitation setup, and even more could be done by concatenating more than one

likelihood. For instance, not only predicting where and when landslides may occur but also jointly predicting how large they may be.

Data Availability Statement

The modeling procedure was conducted in R. The codes are available at the Zenodo repository in Moreno (2024). The landslide inventory can be accessed from Iadanza et al. (2021b). The hourly precipitation data from the INCA data set is available in GeoSphere Austria (2021). The environmental data sets (lithological map, land cover, terrain model) can be accessed from the open geodatabase of the Autonomous Province of South Tyrol (Geo-Browser, 2024). The INCA data set and related environmental data sets are primarily accessible in German. Direct access to precipitation fields of the INCA data set is provided via https://public.hub.geosphere.at/public/datahub.html?id=inca-v1-1h-1km/filelisting&prefix=/RR/. For environmental data sets, we recommend using the search terms "DGM 2.5 m" for the terrain model, "*Geologische Informationen*" for the lithological map, and "*Bodenbedeckung Corine*" for land cover data in the indicated platform.

Acknowledgments

The research that led to these results is related to the PROSLIDE project (https://www.mountainresearch.at/proslide/), which received funding from the research program Research Südtirol/Alto Adige 2019 of the autonomous province of Bolzano. We thank the Faculty of Geo-information Science and Earth Observation (ITC)–University of Twente for covering the open-access publication fees. We thank Dr. Serkan Girgin for his support in using the CRIB platform. We thank the Office for Meteorology and Avalanche Prevention, especially Mauro Tollardo, for supporting and providing the data. We thank the provincial Office for Geology and Building Materials Testing for assisting in preparing landslide data. Finally, we thank Robert Emberson and the two anonymous reviewers for their valuable feedback, which helped improve the quality of this work. This research was supported by the Autonomous Province of Bolzano (Grant 9/34), the Faculty of Geo-information Science and Earth Observation (ITC–UTWENTE), and the Biostatistics and Spatial Processes unit (INRAE).

References

Ahmed, M., Tanyas, H., Huser, R., Dahal, A., Titti, G., Borgatti, L., et al. (2023). Dynamic rainfall-induced landslide susceptibility: A step towards a unified forecasting system. *International Journal of Applied Earth Observation and Geoinformation*, *125*, 103593. https://doi.org/10.1016/j.jag.2023.103593

Aleotti, P., & Chowdhury, R. (1999). Landslide hazard assessment: Summary review and new perspectives. *Bulletin of Engineering Geology and the Environment*, *58*(1), 21–44. https://doi.org/10.1007/s100640050066

Alvioli, M., Loche, M., Jacobs, L., Grohmann, C. H., Abraham, M. T., Gupta, K., et al. (2024). A benchmark dataset and workflow for landslide susceptibility zonation. *Earth-Science Reviews*, *258*, 104927. https://doi.org/10.1016/j.earscirev.2024.104927

Autonomous Province of South Tyrol. (2021). South Tyrol in figures. Provincial statistics institute. Retrieved from https://astat.provinz.bz.it/downloads/Siz_2021-eng(7).pdf

Bajni, G., Camera, C. A., & Apuani, T. (2023). A novel dynamic rockfall susceptibility model including precipitation, temperature and snowmelt predictors: A case study in Aosta Valley (Northern Italy). *Landslides*, *20*(10), 1–24. https://doi.org/10.1007/s10346-023-02091-x

Bogaard, T. A., & Greco, R. (2016). Landslide hydrology: From hydrology to pore pressure. *WIREs Water*, *3*(3), 439–459. https://doi.org/10.1002/wat2.1126

Böhner, J., & Selige, T. (2006). Spatial prediction of soil attributes using terrain analysis and climate regionalisation.

Bolker, B. M., Brooks, M. E., Clark, C. J., Geange, S. W., Poulsen, J. R., Stevens, M. H. H., & White, J. S. S. (2009). Generalized linear mixed models: A practical guide for ecology and evolution. *Trends in Ecology and Evolution*, *24*(3), 127–135. https://doi.org/10.1016/J.TREE.2008.10.008

Bornaetxea, T., Rossi, M., Marchesini, I., & Alvioli, M. (2018). Effective surveyed area and its role in statistical landslide susceptibility assessments. *Natural Hazards and Earth System Sciences*, *18*(9), 2455–2469. https://doi.org/10.5194/nhess-18-2455-2018

Brenning, A. (2012). Spatial cross-validation and bootstrap for the assessment of prediction rules in remote sensing: The R package sperrorest. In *2012 IEEE international geoscience and remote sensing symposium* (pp. 5372–5375).

Brenning, A., Schratz, P., & Herrmann, T. (2022). sperrorest: Perform spatial error estimation and variable importance assessment (version 3.0.5) [Computer Software]. https://cran.r-project.org/web/packages/sperrorest/index.html

Brunetti, M. T., Peruccacci, S., Rossi, M., Luciani, S., Valigi, D., & Guzzetti, F. (2010). Rainfall thresholds for the possible occurrence of landslides in Italy. *Natural Hazards and Earth System Sciences*, *10*(3), 447–458. https://doi.org/10.5194/nhess-10-447-2010

Bryce, E., Castro-Camilo, D., Dashwood, C., Tanyas, H., Ciurean, R., Novellino, A., & Lombardo, L. (2024). An updated landslide susceptibility model and a log-Gaussian Cox process extension for Scotland. *Landslides*, *22*(2), 517–535. https://doi.org/10.1007/s10346-024-02368-9

Budimir, M. E. A., Atkinson, P. M., & Lewis, H. G. (2015). A systematic review of landslide probability mapping using logistic regression. *Landslides*, *12*(3), 419–436. https://doi.org/10.1007/s10346-014-0550-5

Caleca, F., Confuorto, P., Raspini, F., Segoni, S., Tofani, V., Casagli, N., & Moretti, S. (2024). Shifting from traditional landslide occurrence modeling to scenario estimation with a "glass-box" machine learning. *The Science of the Total Environment*, *950*, 175277. https://doi.org/10.1016/j.scitotenv.2024.175277

Camera, C. A. S., Bajni, G., Corno, I., Raffa, M., Stevenazzi, S., & Apuani, T. (2021). Introducing intense rainfall and snowmelt variables to implement a process-related non-stationary shallow landslide susceptibility analysis. *Science of the Total Environment*, *786*, 147360. https://doi.org/10.1016/J.SCITOTENV.2021.147360

Conrad, O., Bechtel, B., Bock, M., Dietrich, H., Fischer, E., Gerlitz, L., et al. (2015). System for automated geoscientific analyses (SAGA) v. 2.1.4. *Geoscientific Model Development*, *8*(7), 1991–2007. https://doi.org/10.5194/gmd-8-1991-2015

Corominas, J., van Westen, C., Frattini, P., Cascini, L., Malet, J. P., Fotopoulou, S., et al. (2014). Recommendations for the quantitative analysis of landslide risk. *Bulletin of Engineering Geology and the Environment*, *73*(2), 209–263. https://doi.org/10.1007/S10064-013-0538-8/FIGURES/5

Crespi, A., Matiu, M., Bertoldi, G., Petitta, M., & Zebisch, M. (2021). A high-resolution gridded dataset of daily temperature and precipitation records (1980-2018) for Trentino-South Tyrol (north-eastern Italian Alps). *Earth System Science Data*, *13*(6), 2801–2818. https://doi.org/10.5194/ESSD-13-2801-2021

Crosta, G. B., & Frattini, P. (2003). Distributed modelling of shallow landslides triggered by intense rainfall. *Natural Hazards and Earth System Sciences*, *3*(1/2), 81–93. https://doi.org/10.5194/nhess-3-81-2003

Crozier, M. J. (1986). *Landslides: Causes, consequences and environment*. Croom Helm. Retrieved from https://books.google.it/books?id=0Rs-AAAAIAAJ

Dahal, A., Tanyas, H., & Lombardo, L. (2024). Full seismic waveform analysis combined with transformer neural networks improves coseismic landslide prediction. *Communications Earth & Environment*, *5*(1), 1–11. https://doi.org/10.1038/s43247-024-01243-8

Dahal, A., Tanyas, H., van Westen, C., van der Meijde, M., Mai, P. M., Huser, R., & Lombardo, L. (2024). Space–time landslide hazard modeling via Ensemble Neural Networks. *Natural Hazards and Earth System Sciences*, *24*(3), 823–845. https://doi.org/10.5194/nhess-24-823-2024

de Vugt, L., Zieher, T., Schneider-Muntau, B., Moreno, M., Steger, S., & Rutzinger, M. (2024). Spatial transferability of the physically based model TRIGRS using parameter ensembles. *Earth Surface Processes and Landforms*, *49*(4), 1330–1347. https://doi.org/10.1002/esp.5770

Dietrich, H., & Böhner, J. (2008). Cold air production and flow in a low mountain range landscape in Hessia (Germany). *Hamburger Beiträge Zur Physischen Geographie Und Landschaftsökologie*, *19*, 37–48.

Elia, L., Castellaro, S., Dahal, A., & Lombardo, L. (2023). Assessing multi-hazard susceptibility to cryospheric hazards: Lesson learnt from an Alaskan example. *The Science of the Total Environment*, *898*, 165289. https://doi.org/10.1016/j.scitotenv.2023.165289

Fang, Z., Tanyas, H., Gorum, T., Dahal, A., Wang, Y., & Lombardo, L. (2023). Speech-recognition in landslide predictive modelling: A case for a next generation early warning system. *Environmental Modelling and Software*, *170*, 105833. https://doi.org/10.1016/j.envsoft.2023.105833

Fell, R., Corominas, J., Bonnard, C., Cascini, L., Leroi, E., & Savage, W. Z. (2008). Guidelines for landslide susceptibility, hazard and risk zoning for land use planning. *Engineering Geology*, *102*(3–4), 83–84. https://doi.org/10.1016/J.ENGGEO.2008.03.009

Felsberg, A., Poesen, J., Bechtold, M., Vanmaercke, M., & De Lannoy, G. J. M. (2022). Estimating global landslide susceptibility and its uncertainty through ensemble modeling. *Natural Hazards and Earth System Sciences*, *22*(9), 3063–3082. https://doi.org/10.5194/nhess-22-3063-2022

Froude, M. J., & Petley, D. N. (2018). Global fatal landslide occurrence from 2004 to 2016. *Natural Hazards and Earth System Sciences*, *18*(8), 2161–2181. https://doi.org/10.5194/nhess-18-2161-2018

Gariano, S. L., Brunetti, M. T., Iovine, G., Melillo, M., Peruccacci, S., Terranova, O., et al. (2015). Calibration and validation of rainfall thresholds for shallow landslide forecasting in Sicily, southern Italy. *Geomorphology*, *228*, 653–665. https://doi.org/10.1016/j.geomorph.2014.10.019

Gariano, S. L., & Guzzetti, F. (2016). Landslides in a changing climate. *Earth-Science Reviews*, *162*, 227–252. https://doi.org/10.1016/J.EARSCIREV.2016.08.011

GeoBrowser. (2024). GeoBrowser maps alto Adige: Maps and digital cartography [Dataset]. https://natura-territorio.provincia.bz.it/it/geobrowser-maps

Geokatalog. (2019). Open geodatabase of the autonomous province of South Tyrol [Dataset]. https://geoportal.buergernetz.bz.it/geodaten.asp

GeoSphere Austria. (2021). INCA stundendaten [Dataset]. *GeoSphere Austria*. https://doi.org/10.60669/6AKT-5P05

Ghaemi, E., Foelsche, U., Kann, A., & Fuchsberger, J. (2021). Evaluation of Integrated Nowcasting through Comprehensive Analysis (INCA) precipitation analysis using a dense rain-gauge network in southeastern Austria. *Hydrology and Earth System Sciences*, *25*(8), 4335–4356. https://doi.org/10.5194/hess-25-4335-2021

Girgin, S. (2021). Using FOSS to develop and operate a geospatial computing platform. https://doi.org/10.5281/zenodo.6025282

Glade, T., Anderson, M., & Crozier, M. J. (2012). Landslide hazard and risk. In *Landslide hazard and risk*. Wiley Blackwell. https://doi.org/10.1002/9780470012659

Goetz, J., Brenning, A., Marcer, M., & Bodin, X. (2018). Modeling the precision of structure-from-motion multi-view stereo digital elevation models from repeated close-range aerial surveys. *Remote Sensing of Environment*, *210*, 208–216. https://doi.org/10.1016/j.rse.2018.03.013

Goetz, J., Brenning, A., Petschko, H., & Leopold, P. (2015). Evaluating machine learning and statistical prediction techniques for landslide susceptibility modeling. *Computers and Geosciences*, *81*, 1–11. https://doi.org/10.1016/j.cageo.2015.04.007

Goldsmith, J., Scheipl, F., Huang, L., Wrobel, J., Di, C., Gellar, J., et al. (2024). *Refund: Regression with functional data* (version 0.1-35) [Computer Software]. https://cran.r-project.org/web/packages/refund/index.html

Gómez, D., Aristizábal, E., García, E. F., Marín, D., Valencia, S., & Vásquez, M. (2023). Landslides forecasting using satellite rainfall estimations and machine learning in the Colombian Andean region. *Journal of South American Earth Sciences*, *125*, 104293. https://doi.org/10.1016/j.jsames.2023.104293

Greco, R., Marino, P., & Bogaard, T. A. (2023). Recent advancements of landslide hydrology. *WIREs Water*, *10*(6), e1675. https://doi.org/10.1002/wat2.1675

Guzzetti, F., Gariano, S. L., Peruccacci, S., Brunetti, M. T., Marchesini, I., Rossi, M., & Melillo, M. (2020). Geographical landslide early warning systems. *Earth-Science Reviews*, *200*, 102973. https://doi.org/10.1016/J.EARSCIREV.2019.102973

Guzzetti, F., Reichenbach, P., Cardinali, M., Galli, M., & Ardizzone, F. (2005). Probabilistic landslide hazard assessment at the basin scale. *Geomorphology*, *72*(1–4), 272–299. https://doi.org/10.1016/j.geomorph.2005.06.002

Haiden, T., Kann, A., Wittmann, C., Pistotnik, G., Bica, B., & Gruber, C. (2011). The integrated Nowcasting through Comprehensive Analysis (INCA) System and its validation over the eastern alpine region. *Weather and Forecasting*, *26*(2), 166–183. https://doi.org/10.1175/2010WAF2222451.1

Hosmer, D. W., Lemeshow, S., & Sturdivant, R. X. (2013). *Applied logistic regression* (3rd ed., pp. 1–510). Applied Logistic Regression. https://doi.org/10.1002/9781118548387

Iadanza, C., Trigila, A., Starace, P., Dragoni, A., Biondo, T., & Roccisano, M. (2021a). IdroGEO: A collaborative web mapping application based on REST API services and open data on landslides and floods in Italy. *ISPRS International Journal of Geo-Information*, *10*(2), 89. https://doi.org/10.3390/ijgi10020089

Iadanza, C., Trigila, A., Starace, P., Dragoni, A., Biondo, T., & Roccisano, M. (2021b). IdroGEO: A collaborative web mapping application based on REST API services and open data on landslides and floods in Italy (No. 2) [Dataset]. *Multidisciplinary Digital Publishing Institute*. https://idrogeo.isprambiente.it/app/page/open-data

IPCC, B. (Ed.) (2022)., *Climate change 2022: Impacts, adaptation and vulnerability. Contribution of working group II to the sixth assessment report of the*. Intergovernmental Panel on Climate Change.

Jakob, M. (2022). Chapter 14—Landslides in a changing climate. In T. Davies, N. Rosser, & J. F. Shroder (Eds.), *Landslide hazards, risks, and disasters* (2nd ed., pp. 505–579). Elsevier. https://doi.org/10.1016/B978-0-12-818464-6.00003-2

Kirschbaum, D., Stanley, T., & Zhou, Y. (2015). Spatial and temporal analysis of a global landslide catalog. *Geomorphology*, *249*, 4–15. https://doi.org/10.1016/J.GEOMORPH.2015.03.016

Knevels, R., Petschko, H., Proske, H., Leopold, P., Maraun, D., & Brenning, A. (2020). Event-based landslide modeling in the Styrian basin, Austria: Accounting for time-varying rainfall and land cover. *Geosciences*, *10*(6), 217. https://doi.org/10.3390/GEOSCIENCES10060217

Kuo, C.-Y., Lin, S.-E., Chen, R.-F., Hsu, Y.-J., Chang, K.-J., Lee, S.-P., et al. (2021). Occurrences of deep-seated creeping landslides in accordance with hydrological water storage in catchments. *Frontiers in Earth Science*, *9*. https://doi.org/10.3389/feart.2021.743669

Lambert, D. (1992). Zero-inflated Poisson regression, with an application to defects in manufacturing. *Technometrics*, *34*(1), 1–14. https://doi.org/10.2307/1269547

Lim, J., Santinelli, G., Dahal, A., Vrieling, A., & Lombardo, L. (2024). An ensemble neural network approach for space–time landslide predictive modelling. *International Journal of Applied Earth Observation and Geoinformation*, *132*, 104037. https://doi.org/10.1016/j.jag.2024.104037

Lima, P., Steger, S., & Glade, T. (2021). Counteracting flawed landslide data in statistically based landslide susceptibility modelling for very large areas: A national-scale assessment for Austria. *Landslides*, *18*(11), 3531–3546. https://doi.org/10.1007/s10346-021-01693-7

Lin, Q., Lima, P., Steger, S., Glade, T., Jiang, T., Zhang, J., et al. (2021). National-scale data-driven rainfall induced landslide susceptibility mapping for China by accounting for incomplete landslide data. *Geoscience Frontiers*, *12*(6), 101248. https://doi.org/10.1016/J.GSF.2021.101248

Loche, M., Scaringi, G., Yunus, A. P., Catani, F., Tanyas, H., Frodella, W., et al. (2022). Surface temperature controls the pattern of post-earthquake landslide activity. *Scientific Reports*, *12*(1), 988. https://doi.org/10.1038/s41598-022-04992-8

Lombardo, L., Opitz, T., Ardizzone, F., Guzzetti, F., & Huser, R. (2020). Space-time landslide predictive modelling. *Earth-Science Reviews*, *209*, 103318. https://doi.org/10.1016/j.earscirev.2020.103318

Maraun, D., Knevels, R., Mishra, A. N., Truhetz, H., Bevacqua, E., Proske, H., et al. (2022). A severe landslide event in the Alpine foreland under possible future climate and land-use changes. *Communications Earth & Environment*, *3*(1), 1–11. https://doi.org/10.1038/s43247-022-00408-7

Marra, F., Nikolopoulos, E. I., Creutin, J. D., & Borga, M. (2014). Radar rainfall estimation for the identification of debris-flow occurrence thresholds. *Journal of Hydrology*, *519*(PB), 1607–1619. https://doi.org/10.1016/J.JHYDROL.2014.09.039

Marra, F., Nikolopoulos, E. I., Creutin, J. D., & Borga, M. (2016). Space–time organization of debris flows-triggering rainfall and its effect on the identification of the rainfall threshold relationship. *Journal of Hydrology*, *541*, 246–255. https://doi.org/10.1016/j.jhydrol.2015.10.010

McLean, M. W., Hooker, G., Staicu, A.-M., Scheipl, F., & Ruppert, D. (2014). Functional generalized additive models. *Journal of Computational & Graphical Statistics : A Joint Publication of American Statistical Association, Institute of Mathematical Statistics, Interface Foundation of North America*, *23*(1), 249–269. https://doi.org/10.1080/10618600.2012.729985

Molnar, P., & Burlando, P. (2008). Variability in the scale properties of high-resolution precipitation data in the Alpine climate of Switzerland. *Water Resources Research*, *44*(10). https://doi.org/10.1029/2007WR006142

Monsieurs, E., Dewitte, O., Depicker, A., & Demoulin, A. (2019). Towards a transferable antecedent rainfall—Susceptibility threshold approach for landsliding. *Water*, *11*(11), 2202. https://doi.org/10.3390/w11112202

Moreno, M. (2024). Software. Reproducible results. Functional regression for space-time prediction of precipitation-induced shallow landslides in South Tyrol, Italy (Version v1.0.1) [Computer Software]. *Zenodo*. https://doi.org/10.5281/zenodo.15033257

Moreno, M., Lombardo, L., Crespi, A., Zellner, P. J., Mair, V., Pittore, M., et al. (2024). Space-time data-driven modeling of precipitation-induced shallow landslides in South Tyrol, Italy. *The Science of the Total Environment*, *912*, 169166. https://doi.org/10.1016/j.scitotenv.2023.169166

Moreno, M., Steger, S., Lombardo, L., de Vugt, L., Zieher, T., Rutzinger, M., et al. (2022). Comparing different strategies to incorporate the effectively surveyed area into landslide susceptibility modeling (Nos. ICG2022-563). ICG2022. *Copernicus Meetings*. https://doi.org/10.5194/icg2022-563

Moreno, M., Steger, S., Tanyas, H., & Lombardo, L. (2023). Modeling the area of co-seismic landslides via data-driven models: The Kaikōura example. *Engineering Geology*, *320*, 107121. https://doi.org/10.1016/j.enggeo.2023.107121

Morris, J. S. (2015). Functional regression. *Annual Review of Statistics and Its Application*, *2*(1), 321–359. https://doi.org/10.1146/annurev-statistics-010814-020413

Nadim, F., Kjekstad, O., Peduzzi, P., Herold, C., & Jaedicke, C. (2006). Global landslide and avalanche hotspots. In *Landslides* (Vol. 3(2), pp. 159–173). Springer. https://doi.org/10.1007/s10346-006-0036-1

Niyokwiringirwa, P., Lombardo, L., Dewitte, O., Deijns, A. A. J., Wang, N., Van Westen, C. J., & Tanyas, H. (2024). Event-based rainfall-induced landslide inventories and rainfall thresholds for Malawi. *Landslides*, *21*(6), 1403–1424. https://doi.org/10.1007/s10346-023-02203-7

Nocentini, N., Rosi, A., Segoni, S., & Fanti, R. (2023). Towards landslide space-time forecasting through machine learning: The influence of rainfall parameters and model setting. *Frontiers in Earth Science*, *11*. https://doi.org/10.3389/feart.2023.1152130

Norris, J. E., Stokes, A., Mickovski, S. B., Cammeraat, E., van Beek, R., Nicoll, B. C., & Achim, A. (2008). Slope stability and erosion control: Ecotechnological solutions. *DordrechtSpringer*. https://doi.org/10.1007/978-1-4020-6676-4

Opitz, T., Bakka, H., Huser, R., & Lombardo, L. (2022). High-resolution Bayesian mapping of landslide hazard with unobserved trigger event. *Annals of Applied Statistics*, *16*(3), 1653–1675. https://doi.org/10.1214/21-AOAS1561

Ozturk, U., Bozzolan, E., Holcombe, E. A., Shukla, R., Pianosi, F., & Wagener, T. (2022). How climate change and unplanned urban sprawl bring more landslides. *Nature*, *608*(7922), 262–265. https://doi.org/10.1038/d41586-022-02141-9

Pedersen, E. J., Miller, D. L., Simpson, G. L., & Ross, N. (2019). Hierarchical generalized additive models in ecology: An introduction with mgcv. *PeerJ*, *2019*(5), e6876. https://doi.org/10.7717/PEERJ.6876/SUPP-1

Peiro, Y., Volpe, E., Ciabatta, L., & Cattoni, E. (2024). High resolution precipitation and soil moisture data integration for landslide susceptibility mapping. *Geosciences*, *14*(12), 330. https://doi.org/10.3390/geosciences14120330

Peruccacci, S., Brunetti, M. T., Gariano, S. L., Melillo, M., Rossi, M., & Guzzetti, F. (2017). Rainfall thresholds for possible landslide occurrence in Italy. *Geomorphology*, *290*, 39–57. https://doi.org/10.1016/j.geomorph.2017.03.031

Piacentini, D., Troiani, F., Soldati, M., Notarnicola, C., Savelli, D., Schneiderbauer, S., & Strada, C. (2012). Statistical analysis for assessing shallow-landslide susceptibility in South Tyrol (south-eastern Alps, Italy). *Geomorphology*, *151–152*, 196–206. https://doi.org/10.1016/J.GEOMORPH.2012.02.003

Ramsay, J. O., & Silverman, B. W. (2005). *Functional data analysis*. Springer. https://doi.org/10.1007/b98888

Reichenbach, P., Rossi, M., Malamud, B. D., Mihir, M., & Guzzetti, F. (2018). A review of statistically-based landslide susceptibility models. In *Earth-science reviews* (Vol. 180, pp. 60–91). Elsevier B.V. https://doi.org/10.1016/j.earscirev.2018.03.001

Reiss, P. T., Goldsmith, J., Shang, H. L., & Ogden, R. T. (2017). Methods for scalar-on-function regression. *International Statistical Review = Revue Internationale de Statistique*, *85*(2), 228–249. https://doi.org/10.1111/insr.12163

Schlögel, R., Kofler, C., Gariano, S. L., Campenhout, J. V., & Plummer, S. (2020). Changes in climate patterns and their association to natural hazard distribution in South Tyrol (Eastern Italian Alps). *Scientific Reports 2020*, *10*(1), 1–14. https://doi.org/10.1038/s41598-020-61615-w

Schmaltz, E. M., Van Beek, L. p. h., Bogaard, T. A., Kraushaar, S., Steger, S., & Glade, T. (2019). Strategies to improve the explanatory power of a dynamic slope stability model by enhancing land cover parameterisation and model complexity. *Earth Surface Processes and Landforms*, *44*(6), 1259–1273. https://doi.org/10.1002/esp.4570

Segoni, S., Piciullo, L., & Gariano, S. L. (2018). A review of the recent literature on rainfall thresholds for landslide occurrence. *Landslides*, *15*(8), 1483–1501. https://doi.org/10.1007/S10346-018-0966-4/FIGURES/2

Smith, H. G., Neverman, A. J., Betts, H., & Spiekermann, R. (2023). The influence of spatial patterns in rainfall on shallow landslides. *Geomorphology*, *437*, 108795. https://doi.org/10.1016/j.geomorph.2023.108795

Stanley, T. A., Kirschbaum, D. B., Benz, G., Emberson, R. A., Amatya, P. M., Medwedeff, W., & Clark, M. K. (2021). Data-Driven landslide nowcasting at the global scale. *Frontiers in Earth Science*, *9*, 378. https://doi.org/10.3389/FEART.2021.640043/BIBTEX

Steger, S., Brenning, A., Bell, R., & Glade, T. (2017). The influence of systematically incomplete shallow landslide inventories on statistical susceptibility models and suggestions for improvements. *Landslides*, *14*(5), 1767–1781. https://doi.org/10.1007/s10346-017-0820-0

Steger, S., & Glade, T. (2017). The challenge of "trivial areas" in statistical landslide susceptibility modelling. In M. Mikos, B. Tiwari, Y. Yin, & K. Sassa (Eds.), *Advancing culture of living with landslides* (pp. 803–808). Springer International Publishing.

Steger, S., Mair, V., Kofler, C., Pittore, M., Zebisch, M., & Schneiderbauer, S. (2021). Correlation does not imply geomorphic causation in data-driven landslide susceptibility modelling – Benefits of exploring landslide data collection effects. *The Science of the Total Environment*, *776*, 145935. https://doi.org/10.1016/j.scitotenv.2021.145935

Steger, S., Moreno, M., Crespi, A., Luigi Gariano, S., Teresa Brunetti, M., Melillo, M., et al. (2024). Adopting the margin of stability for space–time landslide prediction – a data-driven approach for generating spatial dynamic thresholds. *Geoscience Frontiers*, *15*(5), 101822. https://doi.org/10.1016/j.gsf.2024.101822

Steger, S., Moreno, M., Crespi, A., Zellner, P. J., Gariano, S. L., Brunetti, M. T., et al. (2023). Deciphering seasonal effects of triggering and preparatory precipitation for improved shallow landslide prediction using generalized additive mixed models. *Natural Hazards and Earth System Sciences*, *23*(4), 1483–1506. https://doi.org/10.5194/nhess-23-1483-2023

Stingl, V., & Mair, V. (2005). Introduzione alla geologia dell'Alto Adige. Provincia Autonoma di Bolzano-Alto-Adige. Retrieved from https://books.google.it/books?id=ei5jMwEACAAJ

Tanyas, H., Rossi, M., Alvioli, M., van Westen, C. J., & Marchesini, I. (2019). A global slope unit-based method for the near real-time prediction of earthquake-induced landslides. *Geomorphology*, *327*, 126–146. https://doi.org/10.1016/j.geomorph.2018.10.022

Tasser, E., Mader, M., & Tappeiner, U. (2003). Effects of land use in alpine grasslands on the probability of landslides. *Basic and Applied Ecology*, *4*(3), 271–280. https://doi.org/10.1078/1439-1791-00153

Thomas, M. A., Collins, B. D., & Mirus, B. B. (2019). Assessing the feasibility of satellite-based thresholds for hydrologically driven landsliding. *Water Resources Research*, *55*(11), 9006–9023. https://doi.org/10.1029/2019WR025577

Trigila, A., Iadanza, C., & Spizzichino, D. (2010). Quality assessment of the Italian Landslide Inventory using GIS processing. *Landslides*, *7*(4), 455–470. https://doi.org/10.1007/s10346-010-0213-0

Wang, N., Cheng, W., Marconcini, M., Bachofer, F., Liu, C., Xiong, J., & Lombardo, L. (2022). Space-time susceptibility modeling of hydro-morphological processes at the Chinese national scale. *Engineering Geology*, *301*, 106586. https://doi.org/10.1016/J.ENGGEO.2022.106586

van Westen, C. J., van Asch, T. W. J., & Soeters, R. (2006). Landslide hazard and risk zonation—Why is it still so difficult? *Bulletin of Engineering Geology and the Environment*, *65*(2), 167–184. https://doi.org/10.1007/S10064-005-0023-0/FIGURES/5

van Westen, C. J., Castellanos, E., & Kuriakose, S. L. (2008). Spatial data for landslide susceptibility, hazard, and vulnerability assessment: An overview. *Engineering Geology*, *102*(3–4), 112–131. https://doi.org/10.1016/J.ENGGEO.2008.03.010

Wicki, A., Lehmann, P., Hauck, C., Seneviratne, S. I., Waldner, P., & Stähli, M. (2020). Assessing the potential of soil moisture measurements for regional landslide early warning. *Landslides*, *17*(8), 1881–1896. https://doi.org/10.1007/s10346-020-01400-y

Wood, S. N. (2017). *Generalized additive models: An introduction with R* (2nd ed.). Chapman and Hall/CRC. https://doi.org/10.1201/9781315370279

Zuur, A. F., Ieno, E. N., Walker, N., Saveliev, A. A., & Smith, G. M. (2009). *Mixed effects models and extensions in ecology with R*. Springer. https://doi.org/10.1007/978-0-387-87458-6